Graph Theory as an Alzheimer's Disease Diagnostic Instrument in the Context of Functional Brain Connectivity

Dragos Stanciu

Master of Science by Research

Neuroinformatics

DTC in Neuroinformatics and Computational Neuroscience

School of Informatics

University of Edinburgh

2014

Abstract

One of the most common causes of dementia is Alzheimer's Disease (AD). Magnetoencephalography (MEG) is a neuroimaging technique that can monitor how neural oscillations are altered in patients suffering from this disorder. Graph theory is a framework that only recently has been applied to the study of structural and Functional Connectivity (FC) in the human brain. This project aims to construct and compare functional connectivity graphs of healthy subjects and of patients suffering from AD and Mild Cognitive Impairment (MCI). The debiased weighted phase lag index is used to quantify phase synchronisation (PS) between MEG sensors. These partial results are used to build FC graphs for each subject. A number of graph features such as clustering coefficients, modularity and small-world (SW) topology are compared between the three groups. Classifiers based on logistic regression and random forests are then trained using the computed graph metrics. Recordings of new subjects are assigned into one of the AD, MCI or control subjects (CS) categories. A data processing pipeline that achieves the above was designed in the course of this project. A decrease of the SW measure in AD networks compared to CS indicates a decline in network organisation. Poor sensitivity and specificity render the classifiers unsuitable in clinical settings.

Acknowledgements

I would like to express my gratitude to my supervisor, Dr Javier Escudero Rodriguez, for his constant support offered during the course of this project. I would also like to thank the collaborators from the Centre for Biomedical Technology at the Technical University of Madrid for providing the data and for their advice on addressing various issues when working with MEG recordings.

Declaration

I declare that this thesis was composed by myself, that the work contained herein is my own except where explicitly stated otherwise in the text, and that this work has not been submitted for any other degree or professional qualification except as specified.

(*Dragos Stanciu*)

Contents

List of Figures

List of Tables

Chapter 1

Introduction

1.1 Motivation

Alzheimer's Disease (AD) is the most frequent cause of dementia (Cummings, 2004). Global costs are expected to have a remarkable growth as predictions show that by the year 2050, 1 out of 85 people will suffer from the disease (Brookmeyer et al., 2007). Mild Cognitive Impairment (MCI) is a key pre-stage of AD (Morris et al., 2001). Early diagnosis of this stage using inexpensive biomarkers would allow a larger number of patients to start treatments in advance. This may significantly delay disease onset (Cummings, 2004).

Network analysis of neurodegenerative disorders is a young research field which has already shown promising results in disease diagnosis and progression (J. Zhou et al., 2010; Rowe et al., 2010). Magnetoencephalography (MEG) is a neuroimaging technique that can help find differences between neural patterns in the diseased brain and healthy brain (Stam, 2010). Graph theory is a well-established framework that has the potential to standardise interpretation of neuroimaging results (Stam, 2010).

Existing results are inconsistent with respect to certain methodologies (Tijms et al., 2013). This piece of research aims to supplement the current AD research literature by employing promising techniques from three areas of interest: signal processing, graph theory and machine learning.

1.2 Objectives

The present data analysis project aimed to answer the following research question:

What are the identifiable differences in functional brain connectivity between populations of AD, MCI and control subjects (CS)?

The partial objectives of the project were defined in the original proposal (Stanciu and Escudero, 2014) as follows:

Signal Processing

Compute correlations between pairs of MEG sensors

Graph Analysis

Compute functional connectivity graphs and graph measures

Classification

Train classifiers using graph measures as features to assign recordings of new subjects in one of the AD, MCI or CS categories

1.3 Achievements

A modular data processing pipeline has been created which is able to take MEG recordings as input and make predictions about which of the AD, MCI or CS groups the signals originated from.

Brain connectivity graphs were created and graph measures were extracted from them. Classifiers were trained on these measures with the purpose of disease prediction.

Statistical analysis showed that for certain pipeline settings, results were not significant. Nevertheless, an easy to customise framework is in place and future methodological refinements should produce better results.

1.4 Outline

- **Chapter 2** contains background research for better understanding of the scope of the project. Brief presentations of AD and MEG are provided in the beginning sections. These are followed by a description of graph theory concepts and a review of recent studies applying graph theory in the context of functional brain connectivity.

- **Chapter 3** describes the signal processing, graph theory and classification stages of the pipeline used to address the research question in Section 1.2. Techniques used for each of the three modules are explained.
- **Chapter 4** presents the results of this project. These are comprised of extracted graph measures, statistical analysis performed on these values and performances of classification methods.
- **Chapter 5** evaluates the findings and discusses project limitations.
- **Chapter 6** compares deliverables with initial project objectives and suggests avenues for future research.

Conclusion

This chapter described why research in AD is important and outlined the project objectives. The next chapter describes key concepts needed for a better appreciation of the research methods used in this project.

Chapter 2

Background

The project involved analysis of brain connectivity graphs computed from MEG recordings. The following chapter depicts background knowledge needed for a better understanding of chosen methodologies.

2.1 Alzheimer's Disease

Increasing evidence points that the accumulation of beta-amyloid (Aβ) plaques in brain tissue is the most likely cause of AD (Cummings, 2004). Neuronal death is believed to be an effect of this increase in plaques. The only precise way of diagnosing AD is by post-mortem examination of cortical tissue, but this is useful only in disease confirmation after death (Khachaturian, 1985). Treatment in earlier phases of the disease can prove beneficial in delaying disorder symptoms. There are four main stages of AD: MCI, Mild and Moderate AD and Severe AD. In the MCI stage, the patient experiences memory loss as a main symptom (Morris et al., 2001). An area of disease diagnostic that shows promising results is represented by neuroimaging biomarkers (Weiner et al., 2013; Filippi and Agosta, 2011; Sperling et al., 2011).

2.2 The Physics of MEG

MEG is a noninvasive neuroimaging technique that measures perturbations occurring in the magnetic field produced by populations of neurons in the brain (Lopes da Silva, 2013). Figure 2.1 shows that magnetic fields are generated by neuronal currents and picked up by the MEG sensors. The main advantage of

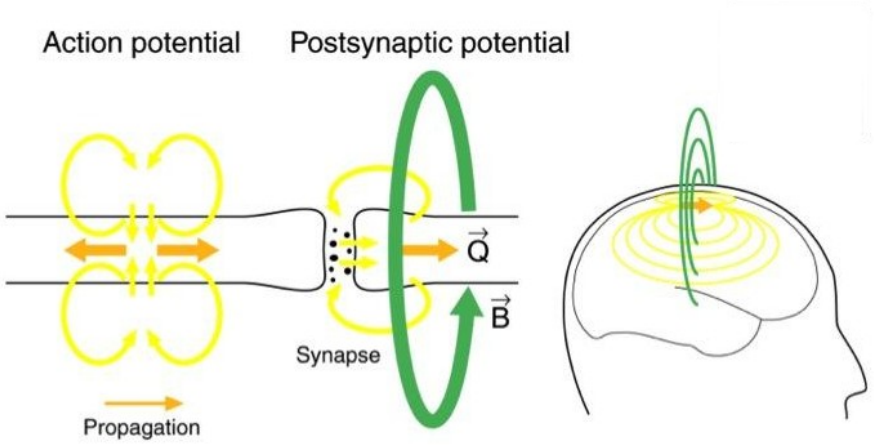

Figure 2.1: Magnetic fields are generated by the electrical activity of neurons (adapted from I-LABS (2014)).

this technology is the high temporal resolution (1-100 Hz). Compared to electroencephalography (EEG) that records electrical impulses at the scalp level, MEG is more precise as magnetic signals suffer less distortion by the scalp and skull (Lopes da Silva, 2013).

The main technological achievement that lies at the foundation of MEG technology is the superconducting quantum interference device (SQUID) (Vrba and Robinson, 2001). This is a very sensitive magnetic detector based on two physical phenomena: superconductivity and quantum tunnelling. It was first used by Cohen (1972) in the context of a single-channel recording. Today's MEG systems can have several hundreds of channels, where each channel corresponds to its own SQUID (Vrba and Robinson, 2001).

There are also several disadvantages of MEG that one should be aware of. In contrast to having high temporal resolution, MEG also has low spatial resolution (order of millimetres or centimetres) (Lopes da Silva, 2013). One of the most pervasive problems in MEG recordings is additive noise. Sources of noise can come from the exterior of the sensor helmet such as cardiac artefacts (Jousmäki and Hari, 1996) and power lines (Keshtkaran and Yang, 2014) or from the interior such as ocular artefacts caused by blinks (Jousmäki and Hari, 1996). These should be minimised in the preprocessing stage of any analysis. The final problem mentioned here is the volume conduction problem that appears when activity from the same source is registered by multiple MEG sensors because of their proximity (Lopes da Silva, 2013).

2.3 Resting-State Synchronisation

Traditionally, MEG signals can be grouped in a number of frequency bands: infraslow (<0.2 Hz), δ (0.2-3.5 Hz), θ (4-7.5 Hz), α and μ (8-13 Hz), β (14-30 Hz), γ (30-90 Hz) and high-frequency oscillations (>90 Hz) (Lopes da Silva, 2013). When populations of neurons share the same firing patterns, neural oscillations arise. Cognitive functions such as memory are believed to rely on these synchronisation patterns between different regions of the brain (Schnitzler and Gross, 2005; Gusnard and Raichle, 2001). The default mode network (DMN) is a network of brain regions that is believed to be active during resting states, when the person is not actively engaged with a certain task (Raichle et al., 2001). Since the introduction of this hypothesis, resting-state studies have been successful in identifying correlations in the same brain regions across subjects (Damoiseaux et al., 2006; Beckmann et al., 2005; Andrews-Hanna et al., 2010).

As AD affects memory, the next step was to try to find differences between the healthy population and patients. Several studies have found significant differences between these groups, where connectivity in AD patients was lower than in control subjects (Stam, B.F. Jones, Manshanden et al., 2006; Greicius et al., 2004; Sheline et al., 2010). The next section introduces graph theory as a relatively new paradigm for brain network analysis (Stam and van Straaten, 2012).

2.4 Connectivity Graphs

Quantitative analysis of brain networks can be obtained using graph theory (Sporns, 2011). Mapping states of biological networks to corresponding graph measures would be instrumental in disease diagnosis and development.

A graph is a structure composed of a set of nodes or vertices and a set of edges. The nodes are connected by the edges. When referring to brain graphs, nodes are mapped to anatomical regions and edges specify a connectivity function. This function can be either structural or functional. The structural function describes the anatomical connections of the nervous system and employs diffusion tensor imaging (DTI) and tractography (D.K. Jones and Leemans, 2011). Functional Connectivity (FC) depicts neurophysiological patterns and is explored using MEG, EEG or MEG technologies. Figure 2.2 shows a high-level scheme of extracting graphs from brain signals. Particular attention should be given to *Step*

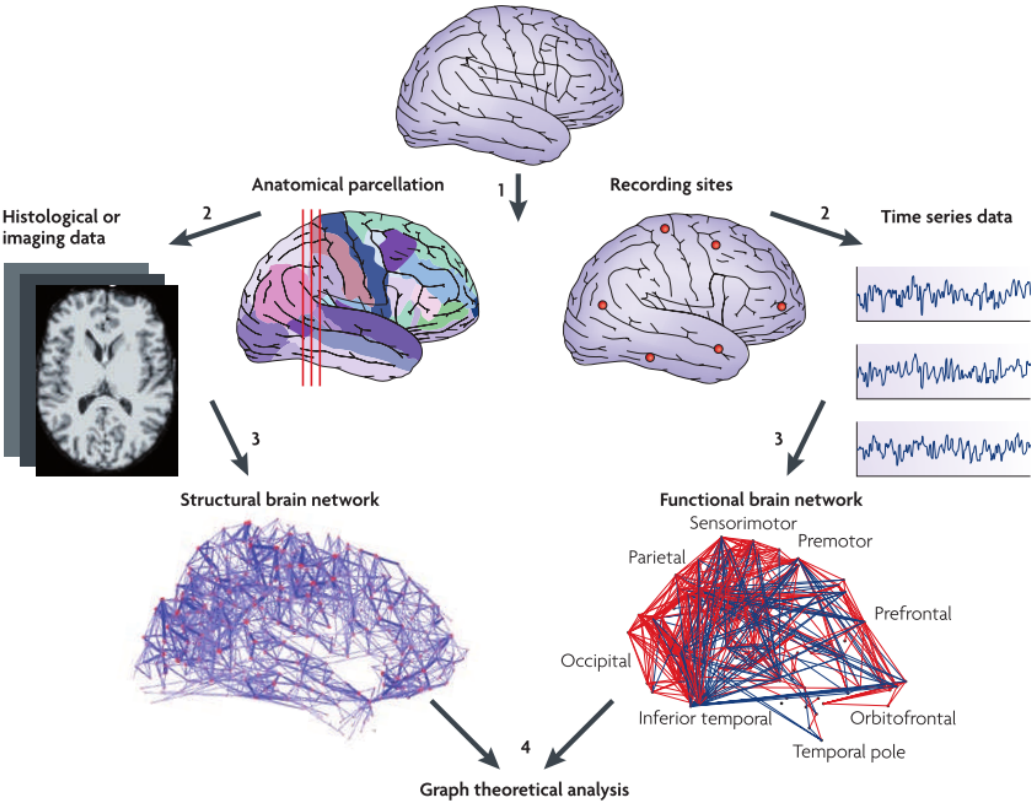

Figure 2.2: Structural and functional brain networks (from E. Bullmore and Sporns (2009)). Step 1 implies identification of graph nodes. This consists of anatomical regions in case of DTI and electrodes in case of EEG or MEG. Step 2 computes a correlation measure between nodes. Step 3 creates an association matrix which holds the correlation strengths between pairs of vertices. Graph measures are computed in the final step.

2, where the association between nodes is computed. In FC, the synchronisation measure just describes statistical correlations between different brain regions and makes no statement about underlying causal effects (Sporns, 2011).

2.5 Graph Theory

This sections aims to introduce a number of graph features relevant to the current study. A comprehensive review of more complex measures can be found in (Rubinov and Sporns, 2010).

Node degree is one of the simplest graph measures. This is given by the number of edges that link a node to the rest of the graph. Another basic graph measure is node centrality. This refers to the number of shortest paths between

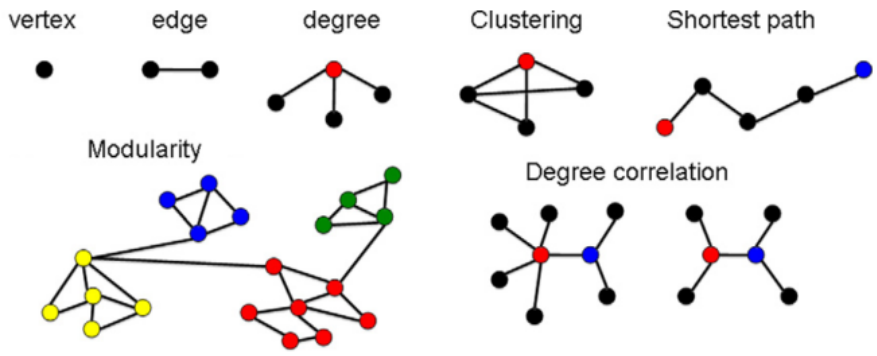

Figure 2.3: Graph measures (adapted from Stam and van Straaten (2012)). The red node in the *degree* graph has a degree of three. For the *shortest path graph*, a minimum of four edges need to be traversed from the red node to the blue node which yields a shortest path of four. Four modules can be seen in the *modularity* graph.

the other pair of nodes in the network that pass through a specific node. High-centrality measures are critical for fast communication. Network hubs are vertices with either high centrality or high degree. Figure 2.3 provides an overview of some of the measures.

The clustering coefficient quantifies local segregation. It refers to how densely connected is a node relative to its neighbours. A high value for this measure indicates that a cluster has been found. The average shortest path length, also called the characteristic path length (L), is calculated by taking the average number of edges in the shortest paths between every node pair in the graph. This measure can also be found under the name of unnormalised path length. The normalised path length is obtained by dividing L by the average path length of a random graph. Random graphs are introduced in the next subsection.

A graph is said to have high modularity if it is formed of subgraphs (modules) that display high intraconnectivity and low interconnectivity (connection between subgraphs).

Watts and Strogatz (1998) introduced the idea of ”small-world” networks which maintain an equilibrium of high clustering and short paths. Brain networks have been hypothesised to posses this property as a consequence of needing to balance infrastructure costs (building neural paths and maintaining them) and high connectivity between brain regions. Fast local computation and integration of information is achieved using the small-world (SW) topology (E. Bullmore and

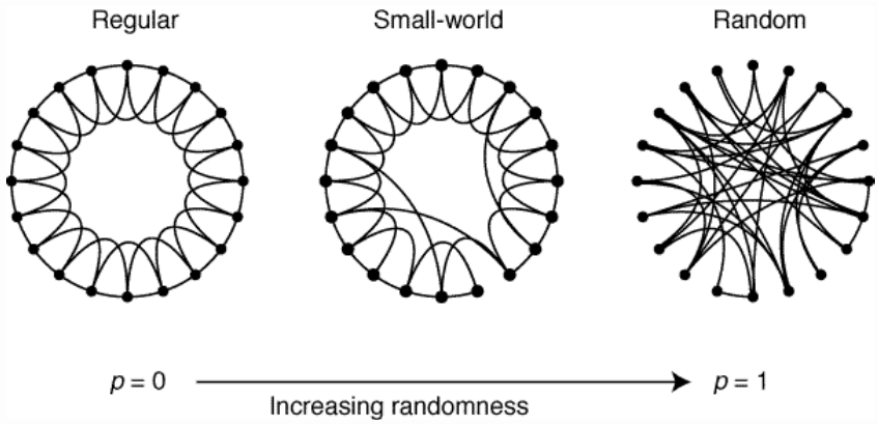

Figure 2.4: Basic network types (from Watts and Strogatz (1998)). Each node of a network is initially connected to its four neighbours. The network is highly clustered and the majority of path lengths between nodes are high. With a probability p, edges are disconnected and reattached to a random node. For p=1, all of the edges will be reconnected which would result in a random network. This network type lost the high clustering property. For value of p between 0 and 1, the network maintains the high clustering quality and depicts small path lengths.

Sporns, 2009). Figure 2.4 compares the SW network with two other networks.

2.6 Network Measures as Biomarkers in AD

Analysis of AD brain networks using graph theory is a relatively recent research endeavour. Two reviews that describe studies that focused exclusively on AD are the ones by He et al. (2009) and Xie and He (2011). Findings of 13 studies that explored graph metrics in AD were listed in the review by Tijms et al. (2013). They found that connectivity decreases in AD graphs. Common graph characteristics were identified by most of the studies, but there are cases where properties are inconsistent across results.

Previous studies reported a decline in clustering coefficients in AD graphs (He et al., 2009; de Haan, van der Flier, Wang et al., 2012). The research by Stam (2004) was one of the first to show that brain networks in healthy subjects have the SW property. All studies reviewed in Tijms et al. (2013) reported that AD networks possess the SW property and 3 out of 13 studies described a decline in the SW value in AD networks, with a possible explanation of path length increase. The reported normalised path lengths in Tijms et al. (2013) were inconsistent.

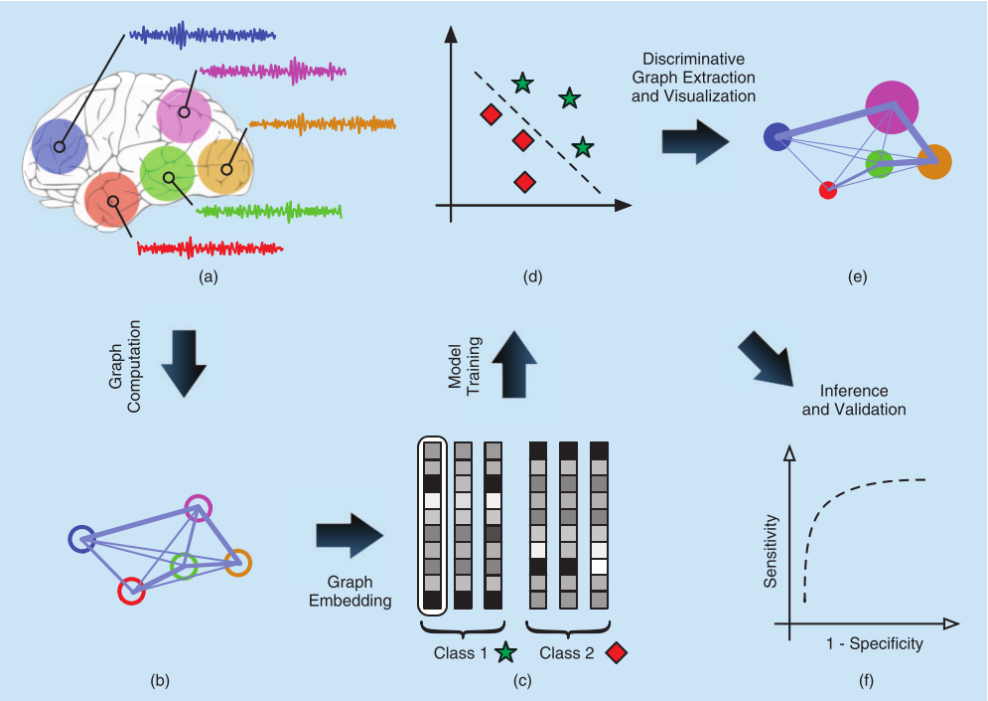

Figure 2.5: Scheme for predictive analysis using brain graphs (from Richiardi et al. (2013)). In a), imaging data is arranged in regions of interest with each region having corresponding time series. b) A graph is computed from the signals in which vertices correspond to brain regions and edges represent correlations between these regions. c) The graphs are organised in vector structures. d) The vectors are used as input for machine learning algorithms. e) Visualisation of interesting patterns is performed so results can be better interpreted. f) Model evaluation is done in the last stage to assess algorithm quality.

The connection between path length and SW property in MCI and AD patients was superficially investigated in the past (Tijms et al., 2013). Modularity in AD was explored in only a single study which found a fewer number of modules in AD networks (de Haan, van der Flier, Koene et al., 2012). In the same study, modularity in the θ band was increased.

Result incompatibilities between studies may be caused by lack of standardised techniques for creating FC graphs (Tijms et al., 2013). Another possible limitation is the small sample sizes employed in the studies. For research that aims to compare three groups such as the one in this project (i.e. AD, MCI and CS), larger sample sizes are needed.

In addition to studies that looked only at comparing network measures in AD, another category distinguishes itself by trying to use machine learning techniques

on computed graph features and subsequently performing classification of individuals (Jie et al., 2014; Chen et al., 2011; L. Zhou et al., 2011). The goal is to bring this research into clinical settings for illness diagnosis purposes. A pipeline schema of a project employing graph analysis in a machine learning setting can be seen in Fig. 2.5.

This project brought together graph analysis of FC networks and classification techniques with the aim of furthering research into network-based diagnosis procedures in AD.

Conclusion

This chapter started by describing AD and why research in this area is important. Afterwards, an overview of MEG was provided as this is the imaging technique used to acquire the data for this project. Lastly, an overview of the state-of-the-art research in graph analysis applied to AD was presented. The next chapter describes the specific techniques used to tackle the problem of finding dissimilarities between AD patients and healthy people.

Chapter 3

Methodology

3.1 Pipeline Overview

Figure 3.1 summarises the data processing pipeline developed for finding differences in FC between the AD, MCI and CS groups. Justifications for chosen methods in different stages are found in corresponding sections.

In the signal processing stage, MEG signals are first filtered into specific bands of interest. The frequency spectrum is then computed for these filtered signals which is then used to perform connectivity analysis between the channels. The connectivity values are saved into matrices which are then used as adjacency matrices in the graph analysis stage. Graph measures are computed from the created networks which are then combined to form feature vectors. Statistical analysis is done to verify differences between each of the CS, MCI and AD groups. The graph feature vectors are finally used as training data for a number of classifiers with the goal of assigning unseen data into one of the studied groups.

3.2 Dataset

The project made use of the same dataset employed in Escudero, Sanei et al. (2011). MEG signals were recorded from a total of 80 subjects in resting-state, with their eyes closed. The data was acquired at the Centre for Biomedical Technology of the Technical University of Madrid using a 148-channel whole-head magnetometer (MAGNES 2500 WH, 4D Neuroimaging). Figure 3.2 shows the layout of the 148 channels. The recordings are five minutes long, collected at a sampling frequency of 169.54 Hz. The mini-mental state examination (MMSE)

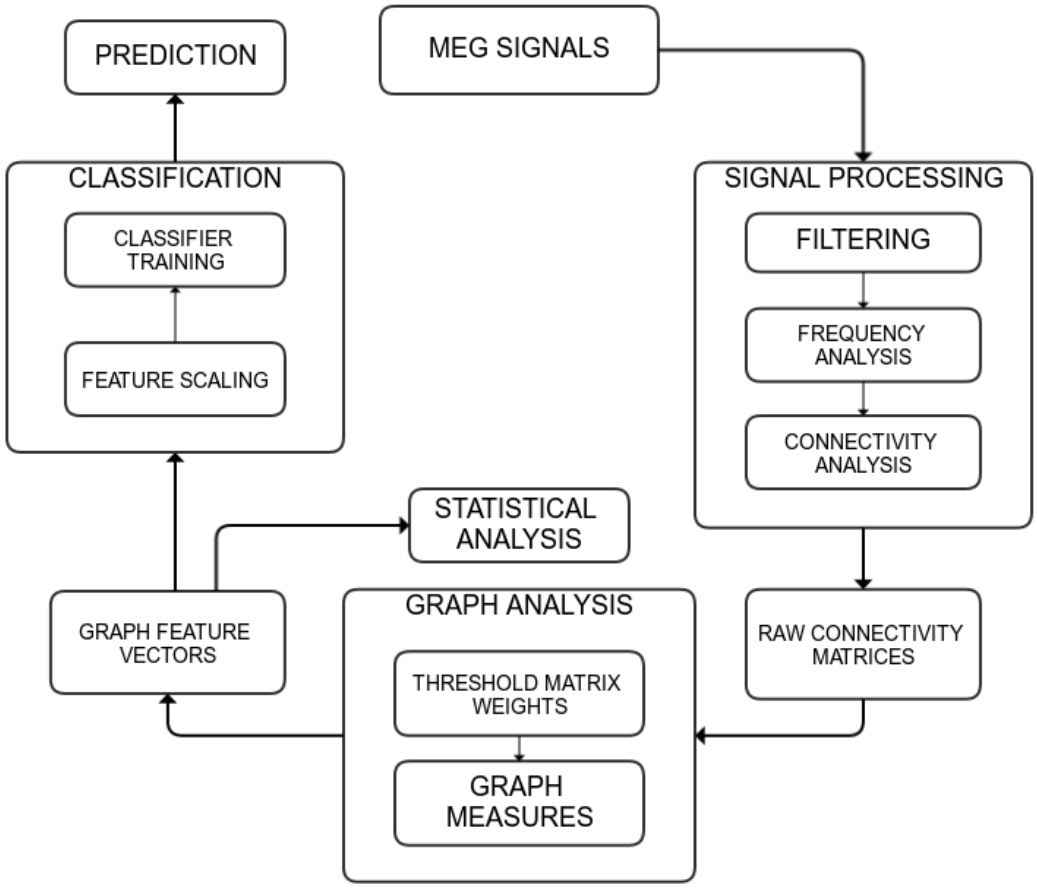

Figure 3.1: Processing pipeline illustrating different stages of data manipulation.

Group	No of subjects	Mean age (± SD)	MMSE
CS	26	71.77 ± 6.38 years	28.88 ± 1.18
MCI	18	74.89 ± 5.57 years	25.67 ± 1.81
AD	36	74.06 ± 6.95 years	18.06 ± 3.36

Table 3.1: Statistics of subjects used in this study

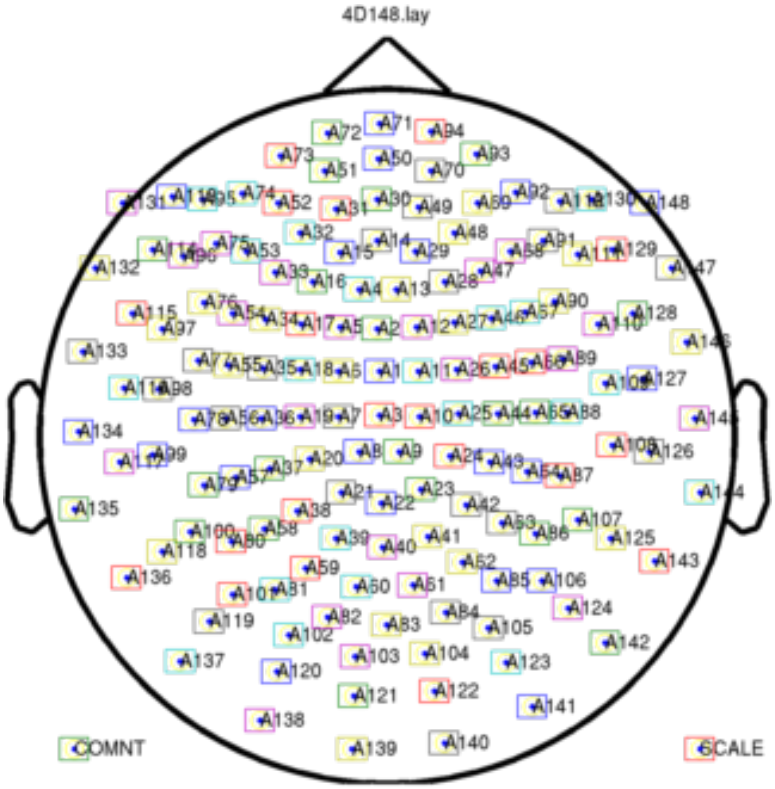

Figure 3.2: Layout of the 148 channels across the subject's head. Image from the FieldTrip toolbox (Oostenveld et al., 2011).

is a test that reflects the cognitive abilities of a subject (M.F. Folstein, S.E. Folstein and McHugh, 1975). Such test scores have also been gathered from all participants. The number of subjects in each group, mean age with standard deviations (SDs) and MMSE scores can be viewed in Table 3.1.

The provided dataset contained two sets of recordings. The first set consisted of the raw MEG recordings which were subjected to routine preprocessing methods (see Escudero, Sanei et al. (2011) for details), while the second set was a subset of the former and was made up of a number of 10s epoch files. These epochs were selected such that obvious ocular artefacts were not present with the help of an amplitude thresholding technique (Hornero et al., 2008). In addition to

this, the cardiac artefact was removed from these recordings with a constrained blind source separation method described in Escudero, Hornero et al. (2011).

The current analysis was done on the second set of recordings cleaned of ocular and cardiac artefacts.

3.3 Signal Processing

This section describes the first part of the processing pipeline which takes as input the 10s epochs and returns connectivity matrices. Figure 3.3 condenses the tasks involved. The FieldTrip Matlab signal processing toolbox was used for implementation (Oostenveld et al., 2011). A significant amount of time was spent developing this component as previous experience with signal processing was absent prior to the start of the project.

3.3.1 Data Preprocessing

Scripts were written to check the integrity of the recordings so that invalid values or other inconsistencies across the files would not affect the next stages of the pipeline. No obvious problems were found with the given data.

3.3.1.1 Baseline Correction

It is important to note that the continuous (DC) offset is present in MEG recordings. As it is desirable for the signals to have a variation around zero, subtraction of the mean registered value across each channel is a common preprocessing step (Gross et al., 2013). As this is an offline analysis, the subtracted mean is computed across the whole epoch so as not to bias the mean, i.e. computing the mean using only the first few samples.

3.3.1.2 Filtering

Filtering is the process by which a signal of interest is extracted by attenuating unwanted components from the original signal (Smith, 1997). The study aimed to inspect FC in the following physiologically relevant bands:

- δ: 0.5 - 4 Hz
- θ: 4 - 8 Hz

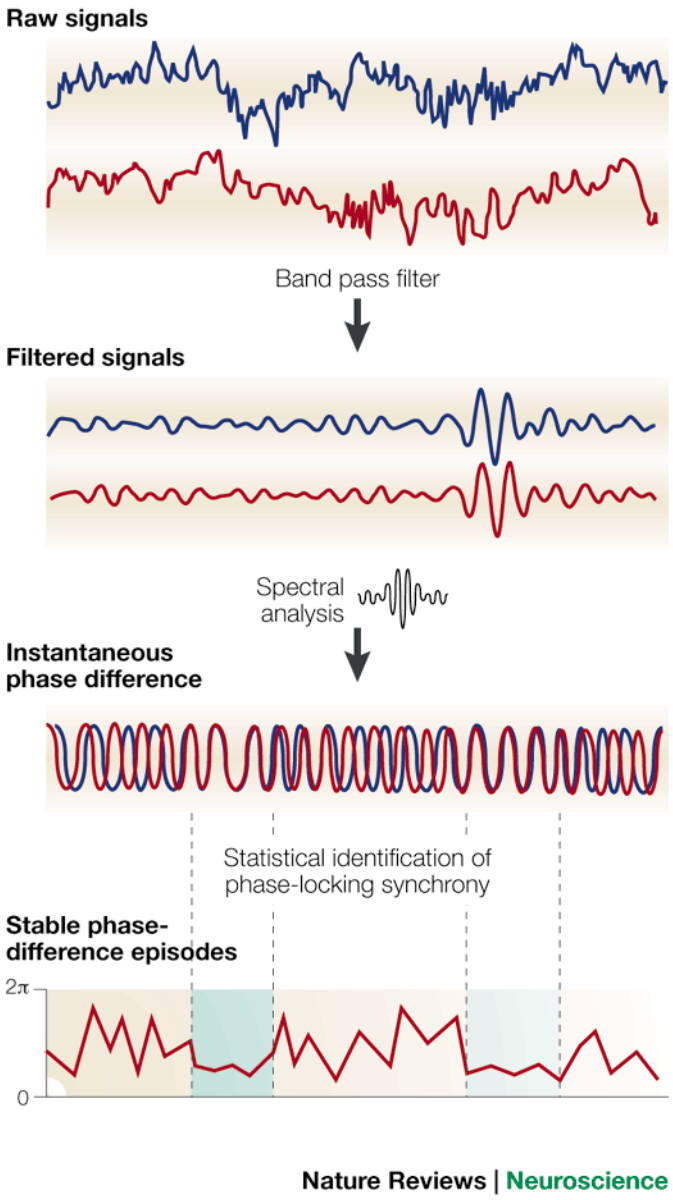

Figure 3.3: Signal processing pipeline (from Varela et al. (2001)). Raw MEG recordings are filtered into the bands of interest. Frequency analysis is used to compute the phase of the signals. Connectivity measures employ this information to establish the level of synchronisation.

- α: 8 - 13 Hz
- β: 13 - 30 Hz
- γ: 30 - 45 Hz

In order to restrict connectivity analysis to a specific band, filtering was performed similarly to the study by Stam, de Haan et al. (2009). This was done using FieldTrip's *ft_preprocessing* function. Epochs were band-pass filtered for each of the above bands using a Finite Impulse Response (FIR) filter which effectively reduced the strength of signals outside the specified frequency intervals. An FIR filter was chosen over an Infinite Impulse Response (IIR) filter as the former exhibits a linear phase response whereas the latter distorts the phase of the signal (Gross et al., 2013). Preserving the phase is crucial for correctly computing phase synchronisation (PS). Although the filter should not in theory affect the phase, the attenuation was applied in both forward and reverse directions as an extra precaution. The filter used a Hamming window, a common and popular windowing function and a filter order of 560 to ensure that the transition from the pass to the stop band is abrupt.

A problem that one should be aware of is the power line interference that affects neural recordings at 50 Hz and harmonic frequencies (Keshtkaran and Yang, 2014). As the highest frequency oscillations studied here are in the interval 30-45 Hz, this does not constitute a problem since the interference is high-pass filtered.

Another problem when performing filtering is the occurrence of edge effects. These arise at the beginning and end of the epoch during the filter pass. The standard method to reduce this problem is padding the signal with extra data. A series of tests were carried out to see if padding the MEG signals would cause a significant difference in the phases of the signals.

In order to better understand how the phase of a signal is obtained, the Hilbert transform is introduced in the next subsection.

3.3.2 Frequency Analysis

3.3.2.1 Hilbert Transform

At the foundation of PS measures lies the instantaneous phase. After filtering the data in a particular frequency band, the instantaneous phase at any given

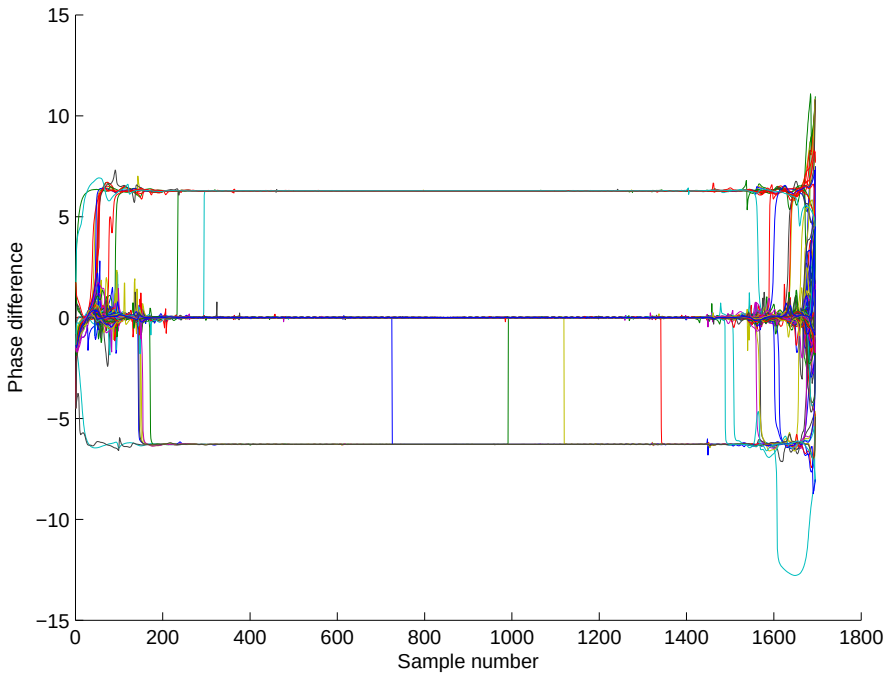

Figure 3.4: Subtracted phases of a padded and unpadded filtered epoch in α band.

point in time can be extracted using the Hilbert transform (Le Van Quyen et al., 2001). The initial time series signal $x(t)$ can be written in analytic form as in Eq. 3.1.

$$z(t) = x(t) + i\tilde{x}(t) \tag{3.1}$$

where $\tilde{x}(t)$ is the Hilbert transform of $x(t)$:

$$\tilde{x}(t) = \frac{1}{\pi} p.v. \int_{-\infty}^{\infty} \frac{x(t')}{t - t'} dt' \tag{3.2}$$

($p.v.$ is the Cauchy principal value). The Hilbert phase is:

$$\Phi_x^H(t) = \arctan \frac{\tilde{x}(t)}{x(t)} \tag{3.3}$$

Unpadded and padded signals were filtered into the bands of interest and the Hilbert transform was computed to obtain the instantaneous phase. The chosen padding was symmetric padding which follows the trend of the signal. In figure 3.4 the phase difference between the padded and unpadded signals for an α band filtered epoch can be observed.

Small fluctuations of the phases occurred at the edges of the signal. This is expected because of edge effects. Visual inspection of similar phase differences in

different epochs revealed similar fluctuations which were deemed insignificant to have an impact on the results. It was decided that signal padding shall not be applied.

3.3.2.2 Frequency Spectrum Estimation

PS measures require phase information which can be obtained from prior computation of the frequency spectrum. This is done by taking the Fourier transform of the given signals, which returns a series of complex numbers where the imaginary part comprises phase information. In order to reduce the amount of noise in the estimation of the frequency spectrum, Welch's periodogram method was employed (Welch, 1967). The original 10s epochs were split into 2s segments with 50% overlap. These segments were then filtered into the bands of interest.

Windowing functions, also called tapers, are multiplied with the data prior to spectral calculation to control frequency smoothing. For frequency bands below 30 Hz (δ - β) it is sufficient to use only a single Hanning taper whereas for analysis in the γ band (30-45 Hz), multiple tapers should be used to improve frequency smoothing (Mitra and Pesaran, 1999; Percival and Walden, 1993). In consequence, for the γ band, discrete prolate spheroidal sequences (Slepian sequences) were used as tapers with a smoothing box of ± 4 Hz (Slepian, 1978; Hoogenboom et al., 2006).

For each 2s segment, spectral density was obtained via FieldTrip's *ft_freqanalysis* function which facilitated tapering and Fourier analysis. The spectral estimates acquired in this stage were then used in connectivity analysis.

3.3.3 Connectivity Analysis

Connectivity measures try to quantify the degree of coupling between two signals. In the context of brain connectivity, these methods can be classified in two main categories: directed measures, which try to infer causal interactions between brain regions, and undirected measures which state the observed correlations (Friston, 1994). As the goal of the project was to find differences in brain synchronisation of patients and controls during resting-state, where no particular causal interactions are sought, an undirected connectivity measure is a natural choice (Fallani et al., 2014). The next step was to explore the available options and choose the ones most likely to yield positive results. In the past years, a

series of methods were developed to address issues such as volume conduction and noise in recordings (Vindiola et al., 2014). One of the most popular measure is the phase locking value (PLV) developed by Lachaux et al. (1999) which is often used when comparing different measures (Aydore, Pantazis and Leahy, 2013). Another measure is the imaginary component of the coherence (ImC) which is robust to spurious correlations caused by the volume conduction effect (Nolte et al., 2004). A new measure that is gaining popularity is the debiased weighted phase lag index (dWPLI) created by Vinck et al. (2011). The study by Vindiola et al. (2014) compared PLV, ImC and dWPLI using simulations and found none of the measures to perform better than the others. In the present study, care was taken to develop a processing pipeline that would integrate with the FieldTrip toolbox so that different synchrony measures can be used effortlessly. This report presents the results obtained with the dWPLI measure, but other techniques such as the PLV and ImC can be explored.

3.3.3.1 Debiased Weighted Phase Lag Index

The dWPLI is an improved version of the phase lag index (PLI) developed by Stam, Nolte and Daffertshofer (2007). This newer technique aims to solve the problem of the PLI not detecting changes in PS in cases of weak coupling between the signals (Vinck et al., 2011). It is also regarded as a method robust against volume conduction.

$$WPLI \equiv \frac{|E\{\Im\{X\}\}|}{E\{\Im\{X\}\}} = \frac{|E\{|\Im\{X\}|sgn(\Im\{X\})\}|}{E\{|\Im\{X\}|\}} \tag{3.4}$$

where $\Im\{X\}$ is the imaginary component of the cross-spectrum between two signals $x(t)$ and $y(t)$. This measure returns values between 0 and 1, where 0 denotes no synchronisation and 1 indicates synchronisation. The debiased method was used in this study (Vinck et al., 2011). Connectivity between each channel was computed using FieldTrips's *ft_connectivityanalysis* function.

The spectral density estimates computed in the frequency analysis step were used to calculate the connectivity values between all pairs of channels. As the recordings were made with a 148-channel MEG machine, a 148×148 matrix was computed illustrating the connectivity strength between each pair. A cell of this matrix corresponded to the correlation between the channel of the row and the channel of the column on which the cell was located. Employing Welch's

method, intermediate connectivity values were computed for each 10s epoch. The final connectivity matrix of a subject was obtained by averaging the intermediate connectivity matrices across all epochs of a subject. Since the analysis was done for five bands of interest, five connectivity matrices were acquired for each subject. The matrices were then sent to the Graph Analysis module.

3.4 Graph Analysis

This section describes the second part of the processing pipeline which takes as input the connectivity matrices from the signal processing unit and returns graph measures corresponding to the observed connectivity.

3.4.1 Constructing Brain Graphs

The dWPLI connectivity matrices can be regarded as adjacency matrices of graphs modelling the subject's brain network activity for different frequency bands. Each MEG channel can be seen as a node in the brain network, whereas entries in the matrix correspond to the strength between the nodes. For convenience, the connectivity matrix obtained in the previous stage can be written as $W_{N\times N}$, where W is a weighted symmetric matrix since dWPLI is an undirected FC metric. Although there is currently no optimal way of converting functional imaging data to graphs (Stam and Reijneveld, 2007), previous studies have consolidated certain procedures that one should take into account.

In the first instance, it was noticed that some negative values were obtained in the dWPLI matrices. Consulting FieldTrip's documentation, this was normal as negative values denote anticorrelations between signals. The negative entries were replaced by their absolute values, as Fallani et al. (2014) advise. The second step was to filter weak links as environmental noise or volume conduction may generate false correlations (Fallani et al., 2014). A threshold X must be chosen for deciding if an entry w_{ij} in W is to be removed or kept. This threshold can either be an absolute threshold or a density threshold also called proportional threshold (E.T. Bullmore and Bassett, 2011). In the case of a simple absolute threshold, an arbitrary value is chosen which would remove edges when w_{ij} is smaller than that value. This is inappropriate as analysis would be restricted for that specific threshold (E. Bullmore and Sporns, 2009). Using a density threshold, only the top

$X\%$ strongest links within the matrix are preserved. A varying density threshold has higher chances of finding topological differences between the networks in the three groups of interest. Care should be taken when choosing threshold values as filtering all links or keeping most of them would result in worthless analysis (Achard and E. Bullmore, 2007). The five density thresholds chosen for X are the following:

$$X = \{0.05, 0.1, 0.15, 0.2, 0.3\} \tag{3.5}$$

Thresholding each of the five frequency band connectivity matrices for five values produced 25 adjacency matrices per subject. A total of 2000 matrices were obtained as there are 80 subjects in the dataset. Binarisation of the graphs is the step by which links that survived the thresholding process are set to unity and links that need to be removed are set to zero. The resulting matrices are treated as adjacency matrices for binary undirected graphs, where nodes i and j are connected if the w_{ij} entry is one. The motivation behind this step is that most graph measures used in the next stage operate only on binary graphs (Rubinov and Sporns, 2010).

3.4.2 Graph Measures

Five graph features were calculated for each of the 25 brain graphs of a subject. The Brain Connectivity Toolbox (BCT) was used to compute these metrics (Rubinov and Sporns, 2010). Similar to the study by Rudie et al. (2012), the chosen measures for this step were global metrics.

average clustering coefficient (C)

The local clustering coefficient of a node measures how densely connected is a node relative to the node's neighbours (Watts and Strogatz, 1998).

$$C_i = \frac{2e_i}{k_i(k_i - 1)} \tag{3.6}$$

where k_i is the number of neighbours of node i and e_i is the number of edges between all of i's neighbours.

The average clustering coefficient (C) is the sum of the local clustering

coefficients divided by the total number of vertices.

$$\overline{C} = \frac{1}{n}\sum_{i=1}^{n} C_i \tag{3.7}$$

characteristic path length (L)

L is the average number of links in the shortest paths between every node pair in the graph.

$$L = \frac{1}{n(n-1)}\sum_{i\neq j} d(v_i, v_j) \tag{3.8}$$

where $d(v_1, v_2)$ is the shortest distance between node v_1 and node v_2.

global efficiency (GE)

global efficiency (GE) is the average inverse shortest path (Latora and Marchiori, 2001). It is used instead of L when networks have disconnected nodes (Fallani et al., 2014).

$$GE = \frac{1}{n(n-1)}\sum_{i\neq j} d(v_i, v_j)^{-1} \tag{3.9}$$

small-worldness (SW)

The SW index of a graph is defined as follows (Watts and Strogatz, 1998):

$$SW = \frac{\frac{C}{C_{rand}}}{\frac{L}{L_{rand}}} \tag{3.10}$$

where C_{rand} and L_{rand} are the C and L of a random network.

Following the methodology described in Rudie et al. (2012), for each adjacency matrix, the computation of the SW value was performed by generating a number of random networks that respected the number of nodes, node degree and edge distribution of the given adjacency matrix. In the referenced study, 100 random networks were generated for each subject network by disconnecting and randomly rewiring each edge of the given network using BCT's *randmio_und_connected* function. The same method was applied in this study, with the observation that six random networks were generated for each matrix because of available computational resources. The average C and L of the created random networks became C_{rand} and L_{rand} in Eq. 3.10. It is important to note that the *randmio_und_connected* function, as the name suggests, maintains the connectedness property of the input graph. A connected graph is a graph where there is a path from any node to any other node.

modularity (Q)

modularity (Q) quantifies to what extent can a network be divided into clearly separated clusters of nodes (Newman and Girvan, 2004).

$$Q = \sum_{u \in M} \left[e_{uu} - \left(\sum_{v \in M} e_{uv} \right)^2 \right] \tag{3.11}$$

where the graph is divided into nonoverlapping modules M and e_{uv} is the proportion of edges connecting vertices in module u with vertices in module v (Rubinov and Sporns, 2010). For computing this measure, the BCT *modularity_und* function was used. For each graph, the function was executed 100 times as the Q measure employs heuristics which can vary from run to run. The average of the 100 runs was taken as the final Q for that graph.

After this stage, graph features have been computed for each subject, for all thresholds in Eq. 3.5, for each frequency band of interest.

3.5 Statistical Testing

This section describes the statistical significance methods used to compare network measures between the groups.

3.5.1 Functional Data Analysis

The study by Bassett, Nelson, B.a. Mueller et al. (2012) proposed Functional Data Analysis (FDA) to examine differences between schizophrenia patients and healthy controls. FDA is a subfield of statistics used for curve comparison (Ramsay and Silverman, 2005). Each network measure computed in the previous section can be plotted as a curve, where the x axis is the threshold value and the y axis represent the value of the metric.

For between group comparisons, the nonparametric permutation test within FDA can be used as follows: for each network measure, the average curves of AD, MCI and CS groups are computed separately. Two groups, for example AD and CS, are chosen for comparison. The area A between the curves of the chosen groups is calculated as in Eq. 3.12.

$$A = \sum_{i=1}^{5} |y_{AD}(X_i) - y_{CS}(X_i)| \tag{3.12}$$

where i goes through each threshold in Eq. 3.5; y_{AD} and y_{CS} are the mean values of the network measure of all subjects in the AD and CS classes respectively.

Nonparametric permutation testing involves randomly reassigning without replacement the group identity of each subject within the classes chosen for comparison. In the AD and CS example, an AD subject may be assigned to the CS group and vice versa. The average curves of the two created pseudo-groups are then computed and the area A' between these curves is calculated as in Eq. 3.12. The procedure is repeated for $k = 10000$ iterations to compile a set of k A' values. The number of A' values greater than A divided by the number of iterations k yielded the p-value of the true population difference, A.

For each pair of groups (CS-MCI, CS-AD, MCI-AD), FDA was performed for all measures, in all frequency bands.

3.6 Classification

This section describes the last part of the processing pipeline which takes as input the graph measures from the graph analysis stage and uses multiple classification techniques to make predictions about which category a certain set of graph measures comes from.

3.6.1 Data Visualisation

t-Distributed Stochastic Neighbour Embedding (t-SNE) is a dimensionality reduction algorithm that is able to take high-dimensional data as input and produce a 2D or 3D plot of the datapoints (Maaten and Hinton, 2008). It works by converting distances between data samples to probabilities and then attempts to minimise the Kullback-Leibler divergence between the joint probabilities of the initial high-dimensional data and the points in the new space with fewer dimensions. The technique is useful as it can show if samples of different classes can be separable in a linear or nonlinear manner. The t-SNE plot of the Mixed National Institute of Standards and Technology (MNIST) dataset of handwritten digits can be seen in Fig. 3.5. Clusters in t-SNE are a very positive sign and indicate that the data is separable. In this case, the clusters represent the digits.

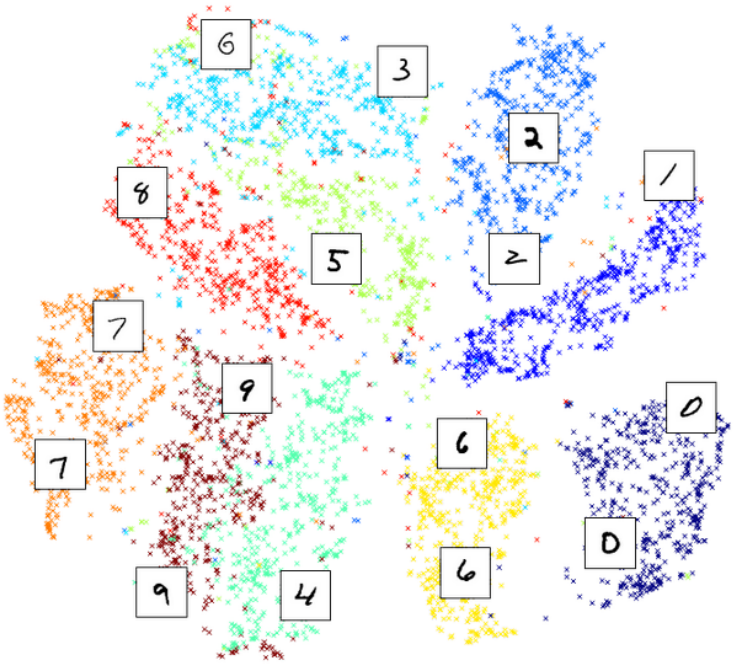

Figure 3.5: t-SNE plot of the MNIST dataset (from Fabisch (2014))

C alpha	L alpha	GE alpha	SW alpha	Q alpha
C beta	L beta	GE beta	SW beta	Q beta
C delta	L delta	GE delta	SW delta	Q delta
C gamma	L gamma	GE gamma	SW gamma	Q gamma
C theta	L theta	GE theta	SW theta	Q theta

Table 3.2: Extracted graph features used for classification.

3.6.2 Feature Extraction

In machine learning, feature extraction is the process by which high dimensional input data to an algorithm is reduced to a set of representative features with the scope of making the required task computationally feasible. This project performed feature extraction in the Graph Analysis section, where each connectivity matrix was summarised by a set of graph metrics. Table 3.2 presents the 25 features computed for each subject, for each threshold.

Given a dataset of N training examples of the form $D = \{(x^n, y^n), i = [1, N]\}$ where x^n is called a training vector and y^n is called a training label, a supervised learning problem aims to approximate a function that maps the input space X to the output space Y. This stage of the project falls in this category of learning as the graph feature vectors have a corresponding y label denoting the AD, MCI

or CS classes.

The following subsections explain the classification algorithms explored during the project.

3.6.3 Logistic Regression

Logistic regression is a type of Generalised Linear Model (GLM) used for classification. It is based on the linear regression model with the modification that the output is passed through a sigmoid function (Murphy, 2012, p. 21). The corresponding model for the binary classification case is found in Eq. 3.13.

$$p(c = 1|\boldsymbol{x} = \sigma(b + \boldsymbol{x}^T \boldsymbol{w}) \tag{3.13}$$

where x is the feature vector, b is the bias of the model and $\boldsymbol{w}$ is the weight vector of the model.

Logistic regression aims to estimate parameters b and $\boldsymbol{w}$ from Eq. 3.13. This is done by maximising the log-likelihood estimation of the data, given in Eq. 3.14.

$$L(\boldsymbol{w}, b) = \sum_{n=1}^{N} c^n \log \sigma(b + \boldsymbol{w}^T \boldsymbol{x}^n) + (1 - c^n) \log \left(1 - \sigma(b + \boldsymbol{w}^T \boldsymbol{x}^n)\right) \tag{3.14}$$

Since in this project there are three possible labels (AD, MCI and CS), a multi-class classification setting is needed. A possible strategy is to use the One-vs-All approach, where three binary classifiers are trained. Each of the three classifiers tries to discriminate if a sample belongs to a class (True) or not (False). The binary classifier treats the samples from the other two classes as negative examples. For new input, the binary classifier with the highest decision function value is chosen as the predicted class.

3.6.4 Random Forests

A random forest is a method based on decision trees (Breiman, 2001). A decision tree is another machine learning technique that tries to predict the target label by building a tree where, at each node, the value of an input feature is examined in order to make a better classification of the input feature vector. Random forests are part of a larger category of ensemble methods which train a series of ”weak classifiers” that when averaged together produce a ”strong classifier”. Each ”weak

classifier" is trained on different subsets of the data (Murphy, 2012, p. 550). For example, the prediction of M trained decision trees is computed as follows:

$$f(x) = \sum_{m=1}^{M} \frac{1}{M} f_m(x) \tag{3.15}$$

where f_m is the m'th tree.

Random forests are a promising technique as they were successfully applied in past studies (Gray et al., 2013; Lehmann et al., 2007).

3.6.5 Other Approaches

Multi-class AdaBoosted Decision Trees (Zhu et al., 2009) were also explored in this project, but were not included in the report due to time constraints. This is also an ensemble method.

3.6.6 Training and Evaluation

The Scikit-learn machine learning library (Pedregosa et al., 2011) was used for training the models on the computed graph features.

3.6.6.1 Feature Standardisation

Prior to classifier training, a common preprocessing step is to standardise the individual features so they have zero mean and unit variance. The mean and standard deviation was computed for each feature. For each feature, the mean is subtracted and the result is divided by the previously computed standard deviation. This was done using the *StandardScaler* class in Scikit-learn using only the training data to prevent "learning" from the testing data.

3.6.6.2 Cross-Validation

It is reminded that five datasets were created with features computed from each threshold in the Graph Analysis stage. Classifiers were run on each dataset separately. In order to ensure generalisability, testing data must not overlap with training data. As the number of samples is small (80 subjects), leave-one-out cross-validation (LOOCV) was employed where the classifier is trained on all data except one feature vector used for testing (Witten and Frank, 2005).

In assessing classifier performance in the context of medical diagnosis, sensitivity and specificity should be taken into account (Lalkhen and McCluskey, 2008). Sensitivity, also known as recall, is the ability of the classifier to identify people having a certain condition. Specificity, also known as the true negative rate, looks at the number of people who do not have the disease and are correctly identified as being healthy.

A measure that takes the above into consideration is the F_1 score:

$$F_1 = 2 \cdot \frac{precision \cdot recall}{precision + recall} \tag{3.16}$$

The score for the F_1 measure lies between 0 and 1, where 0 is the worst possible value and 1 the best.

3.6.6.3 Unbalanced Classes

It was found that classifiers were more biased to assign new samples to the AD group as this class was overrepresented (36 subjects). In order to balance the number of samples of each class, the Synthetic Minority Over-sampling Technique (SMOTE) technique was employed to generate more samples for the MCI and CS classes (Chawla et al., 2002). This technique uses a nearest-neighbour approach to identify samples in the minority class that are close to one another and creates a new sample that lies somewhere between the two existing samples in feature space. The Euclidean distance is used for measuring the distance. A nearest-neighbour value $k = 5$ was used, similar to the original SMOTE paper. The implementation available from Jeschkies (2012) was integrated in the pipeline.

Conclusion

This chapter described the methodological choices for the three main modules of the project: signal processing, graph analysis and classification. The next chapter presents the statistics of the extracted graph measures and the scores obtained in the classification stage.

Chapter 4

Results

This chapter reports the graph measures obtained from the connectivity graphs, results of the statistical analysis and performances of trained classifiers.

4.1 Graph Measures

Figure 4.1 shows the mean graph measure values for each band of interest, for each class. The same plot without the error bars can be seen in Fig. A.1 in Appendix A.

4.2 Statistical Testing

4.2.1 Functional Data Analysis

Statistical analysis using FDA was performed between each pair of classes, for each graph metric and frequency band of interest. The top 20 most significant results (ordered by p-value) are showed in Table 4.1. The full results of the FDA statistical analysis can be found in Appendix B.

4.3 Data Visualisation

4.3.1 t-SNE

The extracted graph features for each threshold were plotted using t-SNE (Maaten and Hinton, 2008). Figures 4.2 to 4.6 show the plots for each threshold. It can be seen that the datapoints of the AD, MCI and CS classes are mixed and no

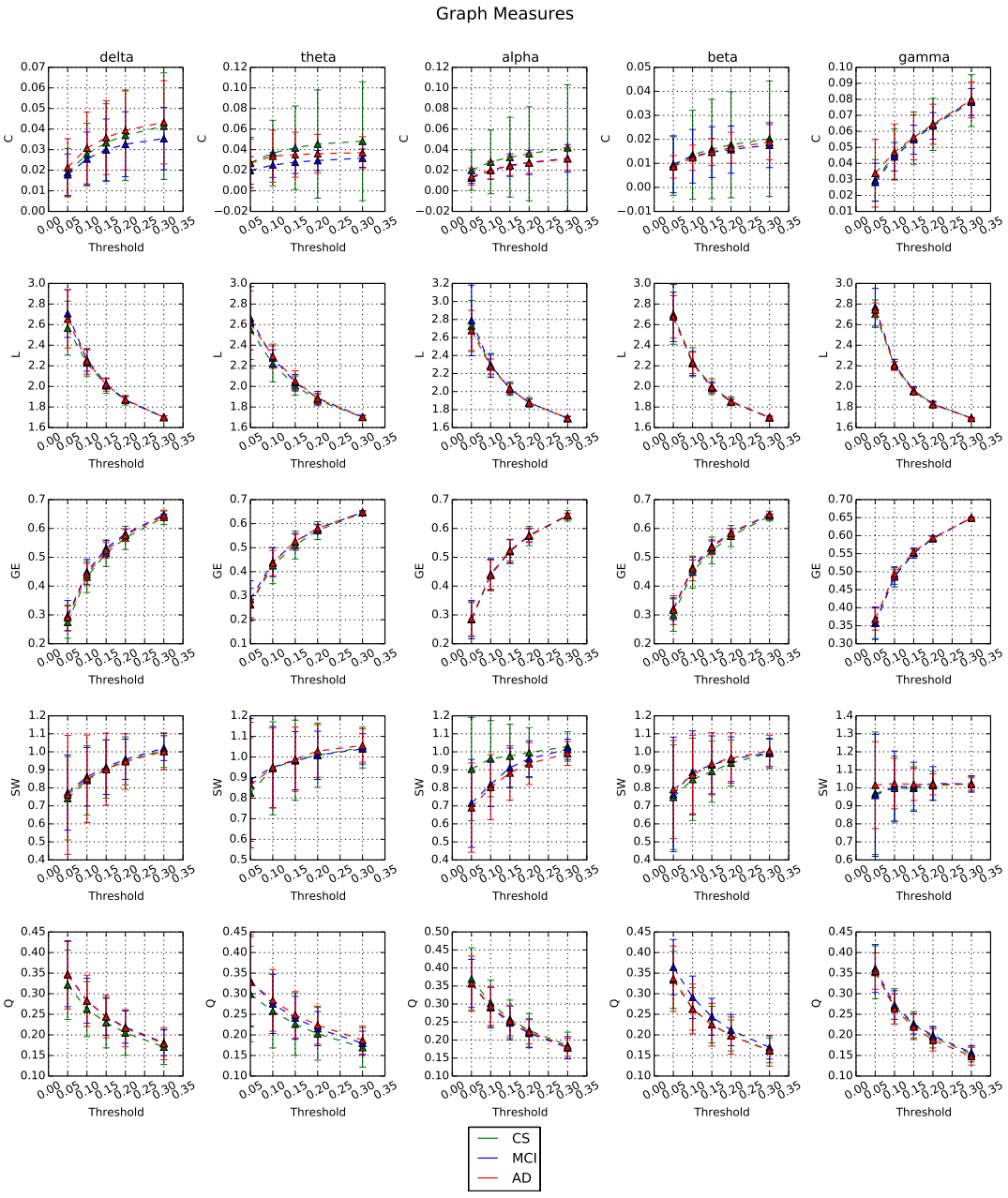

Figure 4.1: Graph measures illustrating mean graph metric curves. Rows represent measures, columns represent frequency bands of interest. For each subplot, the x axis represents the threshold value and the y axis represents the graph measure value. C is the average clustering coefficient, L is the characteristic path length, GE is global efficiency, SW is the small-world measure and Q is modularity.

Measure	**Group A**	**Group B**	**Band**	**p-value**
SW	CS	AD	alpha	0.006
SW	CS	MCI	alpha	0.0657
GE	CS	MCI	delta	0.161
L	CS	MCI	delta	0.1637
Q	CS	MCI	beta	0.1688
L	CS	AD	gamma	0.1691
GE	CS	MCI	beta	0.1868
L	CS	AD	theta	0.1902
Q	MCI	AD	beta	0.1907
Q	CS	AD	theta	0.1912
C	MCI	AD	theta	0.1914
C	CS	MCI	theta	0.1942
GE	CS	AD	gamma	0.2103
C	MCI	AD	delta	0.2203
GE	MCI	AD	gamma	0.2224
L	CS	MCI	theta	0.226
C	CS	AD	alpha	0.2401
GE	CS	AD	beta	0.2445
GE	CS	AD	delta	0.252
Q	CS	AD	delta	0.2991

Table 4.1: Results of the FDA statistics. Top 20 lowest p-values are listed. (see Appendix B for full list.)

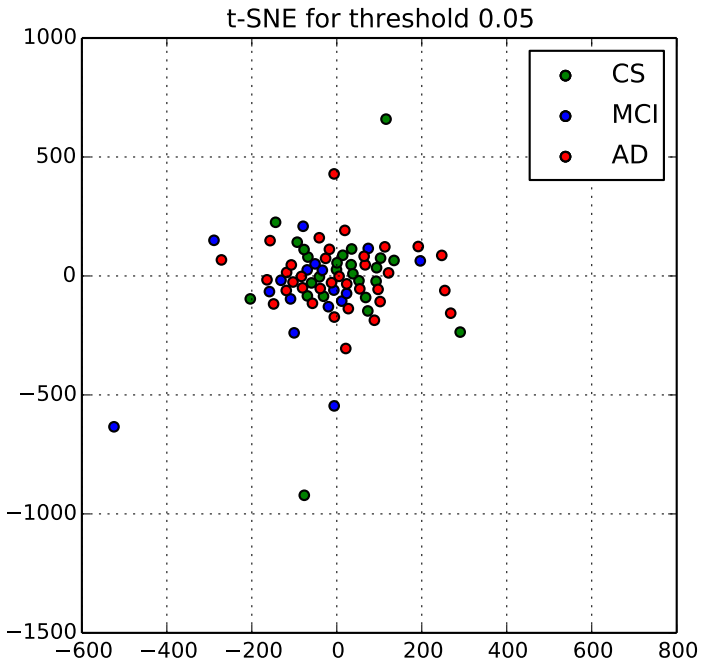

Figure 4.2: t-SNE plot for threshold 0.05.

particular clusters can be discerned. This suggests that the data would be hard to separate.

4.3.2 Box Plots and Parallel Coordinates

Box plots can be used to inspect the variance of the graph measures among the subjects. Figure 4.7 shows the box plot of the features computed when looking at the top 15% strongest links in the connectivity matrices. It can be seen that the most interesting measure is the SW value which shows higher variance compared to other measures. Other measures such as C and GE show large number of outliers which would make it difficult for such metrics to be used for classification. Similar patterns can be seen in the box plots of the other thresholds. These are included in Fig. A.2 to A.5 in Appendix A.

A common way of visualising high-dimensional data is to use parallel coordinates plots. These represent the features of the input data as a set of vertical lines. A data sample is represented as a polyline with vertices on the feature lines. Figure 4.8 shows a parallel coordinate plot for the features of threshold 0.15. The high overlap of the polylines indicates that there is no clear organisation. The

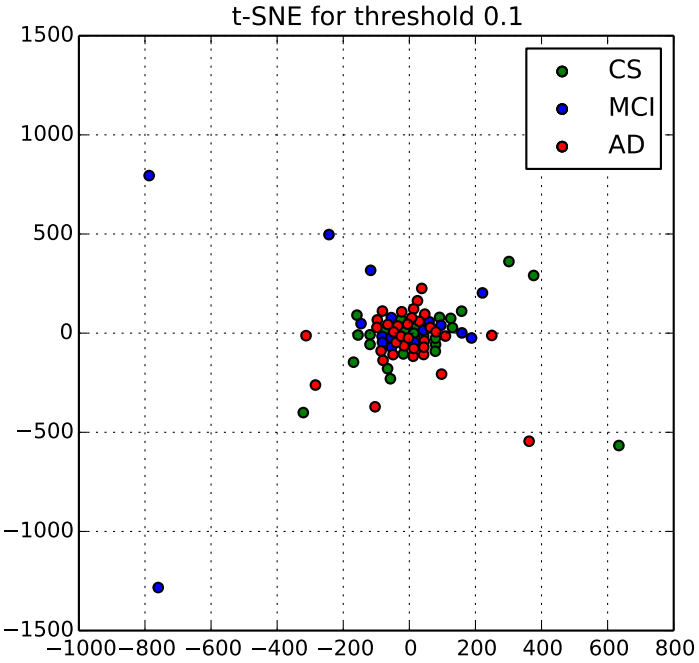

Figure 4.3: t-SNE plot for threshold 0.1.

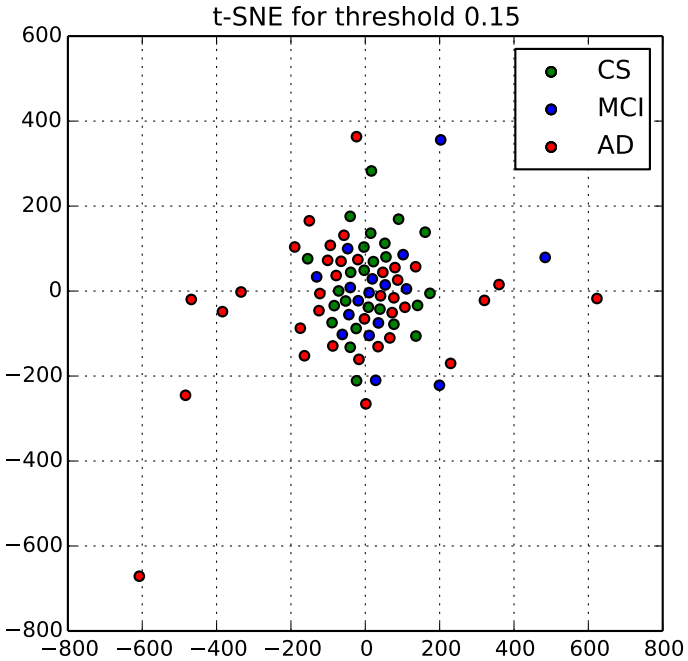

Figure 4.4: t-SNE plot for threshold 0.15.

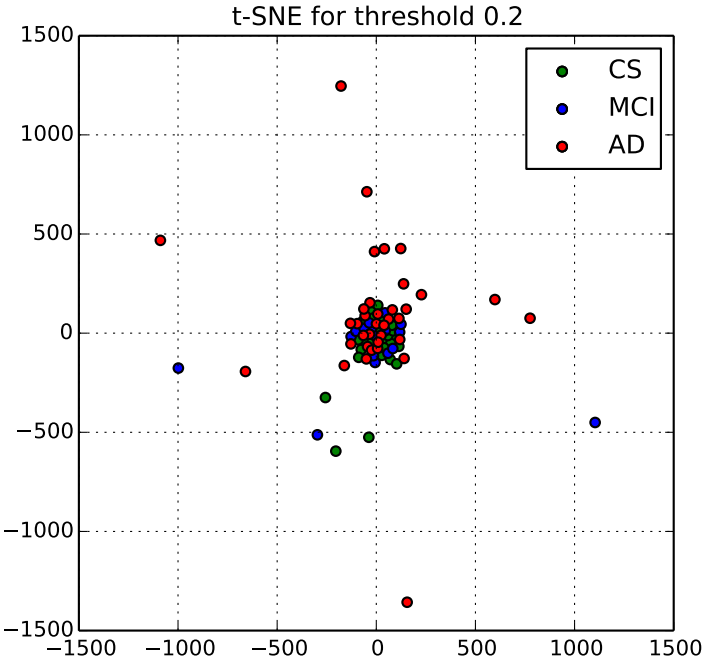

Figure 4.5: t-SNE plot for threshold 0.2.

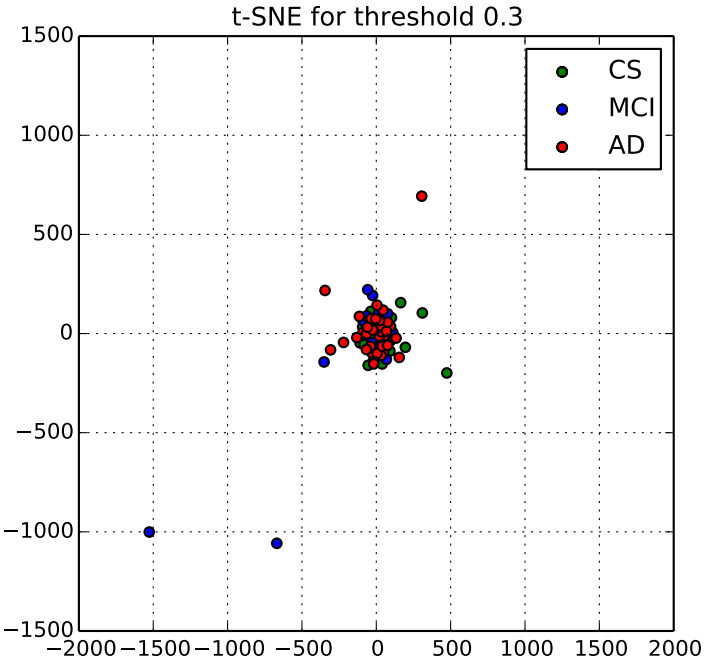

Figure 4.6: t-SNE plot for threshold 0.3.

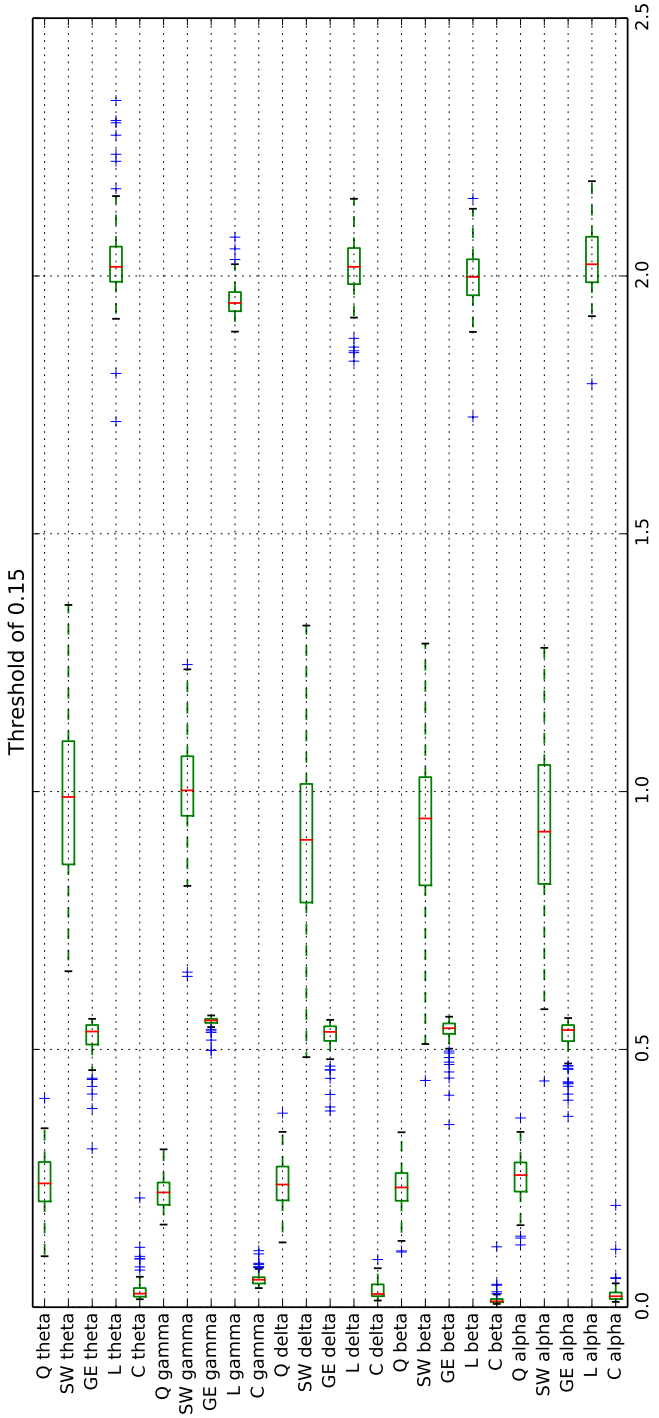

Figure 4.7: Box plot of graph measures for threshold 0.15.

Threshold	LR (original)	LR (SMOTE)	RF (original)	RF (SMOTE)
0.05	Table C.1	Table C.2	Table C.11	Table C.12
0.1	Table C.3	Table C.4	Table C.13	Table C.14
0.15	Table C.5	Table C.6	Table C.15	Table C.16
0.2	Table C.7	Table C.8	Table C.17	Table C.18
0.3	Table C.9	Table C.10	Table C.19	Table C.20

Table 4.2: Confusion matrices lookup table. T is the threshold, LR stands for logistic regression and RF is random forest.

T	LR (original)	LR (SMOTE)	RF (original)	RF (SMOTE)
0.05	0.47	0.57	0.46	0.69
0.1	0.43	0.57	0.39	0.69
0.15	0.41	0.44	0.39	0.69
0.2	0.35	0.5	0.35	0.67
0.3	0.35	0.4	0.44	0.65

Table 4.3: F_1 scores. T is the threshold, LR stands for logistic regression and RF is random forest.

plots for the other thresholds are found in Fig. A.6 to A.9 in Appendix A.

4.4 Classification

In this section, the confusion matrices and F_1 scores of the logistic regression and random forest classifier are reported. The classifiers have been trained on the measures from each threshold separately. In addition, classification with just the original data and with the added SMOTE samples has been performed.

4.4.1 Confusion Matrices

The confusion matrices for each algorithm can be found in Appendix C. A specific matrix can be looked up using Table 4.2.

4.4.2 F_1 Scores

Table 4.3 lists the F_1 scores obtained for the two chosen classifiers.

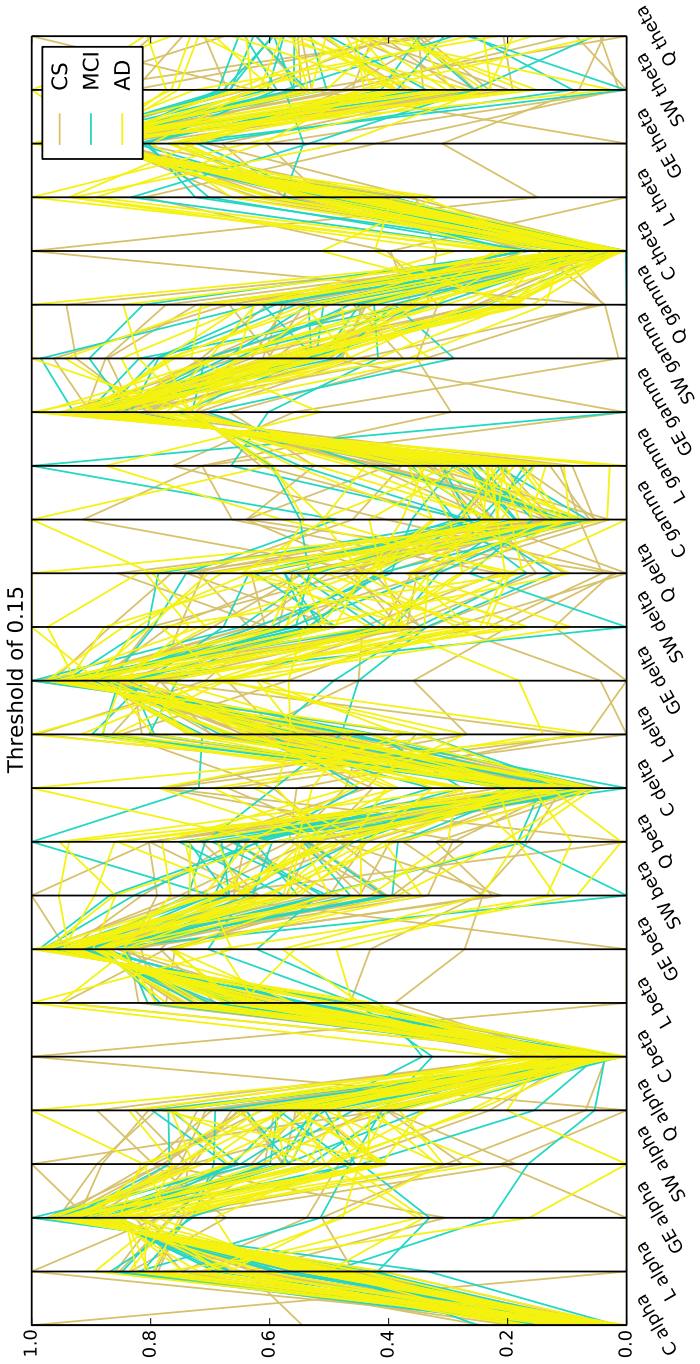

Figure 4.8: Parallel coordinates plot of graph measures for threshold 0.15.

Conclusion

This chapter presented the computed graph measures with afferent statistics. Results of classification into the three groups of interest were also showed. The next chapter examines these results with respect to the initial project objectives.

Chapter 5

Discussion

It is reminded that the main objective that this project set out to achieve was finding the main differences in functional brain connectivity between populations of AD, MCI and CS. This objective was divided in a set of three partial goals composed of a signal processing stage, a graph analysis step and a classification stage.

The first observation that needs to be made is related to the statistical analysis. The only significant result ($p < 0.05$) was for the SW measure when FDA was done between the AD and CS groups in the α band. This supposedly happened because of the AD networks having a topology closer to that of random networks as reported in previous studies (Stam, B.F. Jones, Nolte et al., 2007; Lo et al., 2010; Zhao et al., 2012). This may be due to a decrease in the normalised path length ($\frac{L}{L_{rand}}$), but results are not significant enough to prove this hypothesis.

Previous studies reported that SW networks have a value much higher than unity (Rubinov and Sporns, 2010). The reason behind this is that C is greater than 1 and $\frac{L}{L_{rand}}$ approaches 1. When building the connectivity graphs, with increasing density thresholds, it is expected that SW should decrease and approach unity as more and more edges are added to the graph. In the present study, it can be observed in Fig. 4.1 that SW values start at a low value when small thresholds are used. As weaker links are added to the graphs, SW increases and starts to approach the value of one.

A possible explanation for this strange behaviour is the way the random networks are created when computing SW. For small thresholds (only strongest links are kept), the graph risks of becoming segmented and multiple graph com-

ponents (subgraphs) may emerge. The BCT *randmio_und_connected()* function that generates the random graphs maintains the connectedness property of the input graph. There is a chance that this function might cluster the rewired edges into a single component, which in turn increases the average clustering coefficient for a random graph. A solution for this problem would be to either change how the random graphs are generated or, more conveniently, restrict analysis to thresholds that satisfy the condition that all subject graphs are connected, i.e each subject graph is a single component graph (Rudie et al., 2012). In this case, connectedness refers to the ability of a node to reach any other node in the graph and should not be confused with a fully connected graph where there is a link between every node and every other node in the graph. The creation of random graphs used for comparison is a known problem (Tijms et al., 2013) and studies should specify how these networks are created. The present study identified that caution should be exercised when relying on libraries for random network generation.

The same problem of multiple graph components in the same connectivity network might occur in other measures which might explain the rapid change of the mean curves in Fig. 4.1. Measures such as GE are robust to the problem of isolated nodes in the graph (Latora and Marchiori, 2001; Fallani et al., 2014). In the present results, the measure increases almost uniformly as path lengths decrease with the additions of weaker edges, but no observations can be made about group differences.

The plot of mean graph measures without the error bars found in Appendix A, Fig. A.1 seemed to clearly show that C is higher in CS than either AD or MCI in the θ band, but high within-group variance proved this pattern to be insignificant.

Q was shown by de Haan, van der Flier, Koene et al. (2012) to be smaller in AD networks, but no conclusive observations can be made about the present results.

Classification was known to be a difficult task after the generation of t-SNE plots. Figures 4.2 to 4.6 show that there are no clear clusters of data. This means that the computed graph features are not very structured and separating the classes would be far from trivial. Brief inspection of the confusion matrices in Appendix C reveals that both logistic regression and random forest classifier were biased in predicting AD. The cause of this is the class imbalance problem

and can be solved by training the algorithms with the same number of training samples for each class (Chawla et al., 2002). In this project, the problem was solved using SMOTE by generating new samples for the minority classes. With the new data, both classifier performances improved. A caveat of this method is that the algorithms were essentially partly trained with ”fake data” which does not necessarily reflect data from an actual subject. In consequence, if a study is performing classification, a strong recommendation would be to have an equal number of subjects in each group of interest to avoid the class imbalance problem.

Random forests (Breiman, 2001) have shown promising results considering the low variance in the computed graph measures. Because the random forest is an ensemble method, it is likely that some decision trees were able to correctly identify the interesting features such as SW in the α band which would result in better classification scores of the forest. To the author's best knowledge, this is the first study to apply random forests to graph measures in the context of AD brain networks.

Inspecting the F_1 scores in Table 4.3 shows that classifier performance is better when choosing lower thresholds. The likely explanation for this is that as the threshold is increased, weaker links are added to the network, which do not resemble the true connectivity between the sensors. When the threshold reaches a high-enough value, the graph resembles a random graph and discriminating between groups is in vain.

Although an F_1 score of almost 0.7 seems to indicate a good performance when considering that 1 is the perfect score, this is not enough to allow the random forest to be viable in a clinical setting. It can be seen from the confusion matrices in C.2 that the algorithm incorrectly classifies a large number of CS subjects in the AD and MCI categories. This means that the algorithm has low specificity and high sensitivity which would result in people undergoing unnecessary treatments (Lalkhen and McCluskey, 2008).

Several limitations of this study need to be mentioned. Although this study has a relatively higher sample size than previous studies looking at AD, MCI and CS groups (Tijms et al., 2013), this was not sufficient to gain significant results. It is very likely that changes in methodology would provide different results, but in either case, more data samples are conducive to concluding that certain patterns exist. Similar to any MEG study, noise represents a major concern. Visual inspection of epochs was a priori performed on the dataset to remove

ocular artefacts and constrained blind source separation was used to remove the cardiac artefact (Escudero, Hornero et al., 2011). In the latter case, the same electrocardiogram component was subtracted from the channels of all epochs of a subject. This in theory should preserve the relative phases between the signals, but further analysis which uses the raw MEG signals without the cardiac artefact removal should be performed for comparison. Another source of noise that should be taken into account when interpreting results is volume conduction (Gross et al., 2013). dWPLI is a measure robust to this problem, but spurious correlations are still a possibility. There are also graph threshold values that have not been explored. It may also be beneficial to perform ”windowed thresholding” similar to Bassett, Nelson, B.A. Mueller et al. (2012) to investigate ”weak links” between certain intervals for interesting patterns.

Chapter 6

Conclusions

A complete processing pipeline was built during the course of this highly interdisciplinary project. In the signal processing stage, MEG signals were filtered into the frequency bands of interest, frequency analysis was used for extracting phase information and dWPLI was applied to compute correlations between sensors. In the graph analysis stage, proportional thresholding was used to create five connectivity matrices for each subject. Graph features were computed for each matrix. In the last stage, classification using logistic regression and random forests was performed on the graph metrics.

While the individual modules of the initial pipeline plan were to a certain degree completed, insignificant results were obtained according to statistical testing. The two main problems in the methodological approach are as follows: in the graph analysis stage, there is a clear problem with the generation of random graphs, which in turn affects the SW measure. Further investigation is needed. In the classification stage, the algorithms need to be tweaked so that specificity is increased.

6.1 Future Work

As good classification scores are a natural consequence of good, separable features, it follows that identification of measures and methodologies that return features with significant differences across groups are to be prioritised. Stam, Tewarie et al. (2014) recently put forward a new technique to solve the thresholding problem. He advises using the Minimum Spanning Tree as the basis for computing network measures. This should provide the basis for a more standard procedure

for computing graph metrics. There have been some preliminary results that showed significant results in this project when the PLV connectivity measure was employed in the signal processing stage. Comparison of different connectivity measures is a possible future step. Lastly, there has been a trend for the neuroscience community to shift from sensor analysis to source analysis (Schoffelen and Gross, 2009). This is motivated by the volume conduction problem. Due to time constraints, source analysis was not explored, but a future project may try this approach. Magnetic resonance imaging was not available for this dataset, but recent tools make use of default anatomical maps that can facilitate source reconstruction (Tadel et al., 2011).

Appendix A

Supplementary Figures

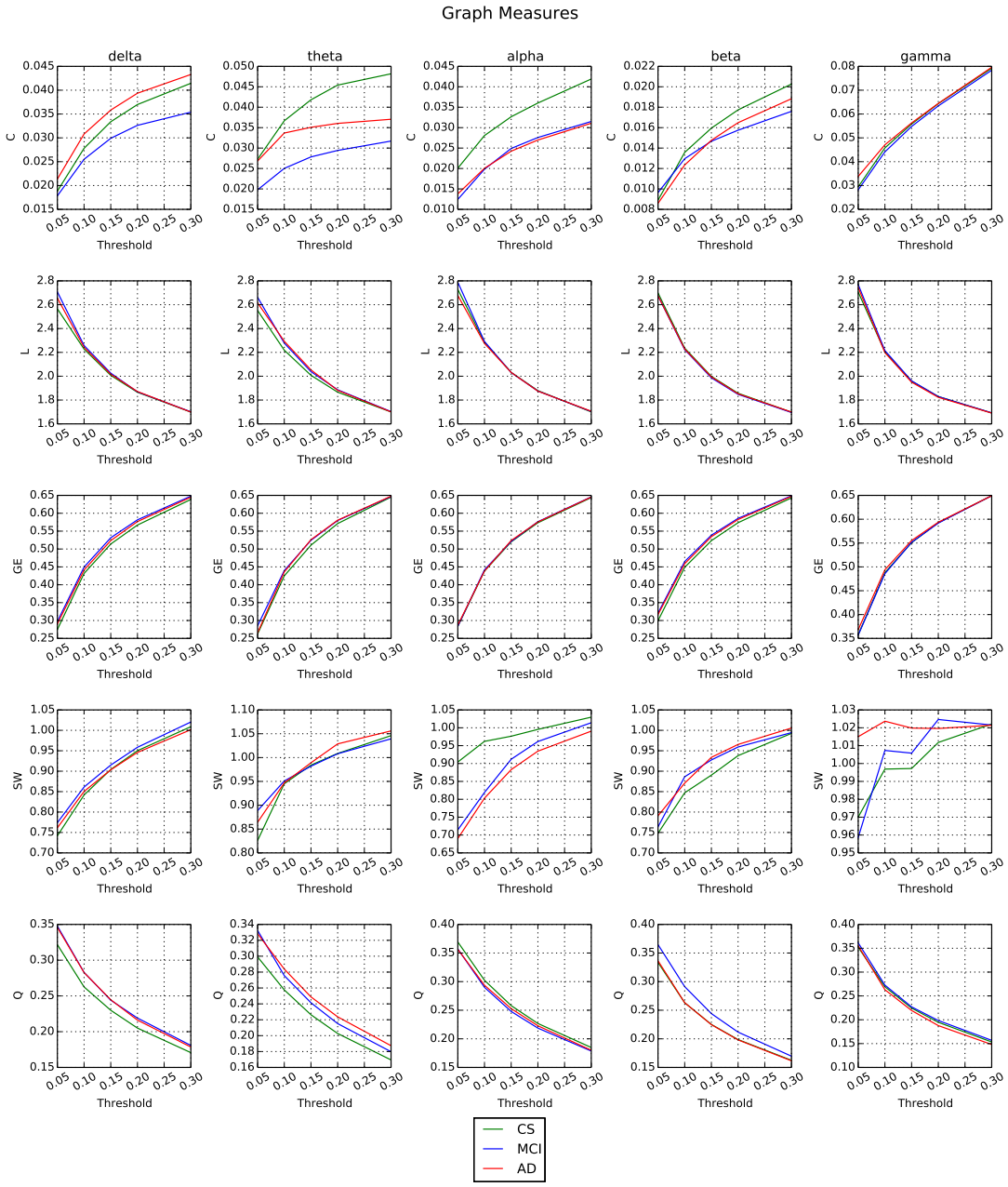

Figure A.1: Graph measures with no error bars illustrating mean graph metric curves.

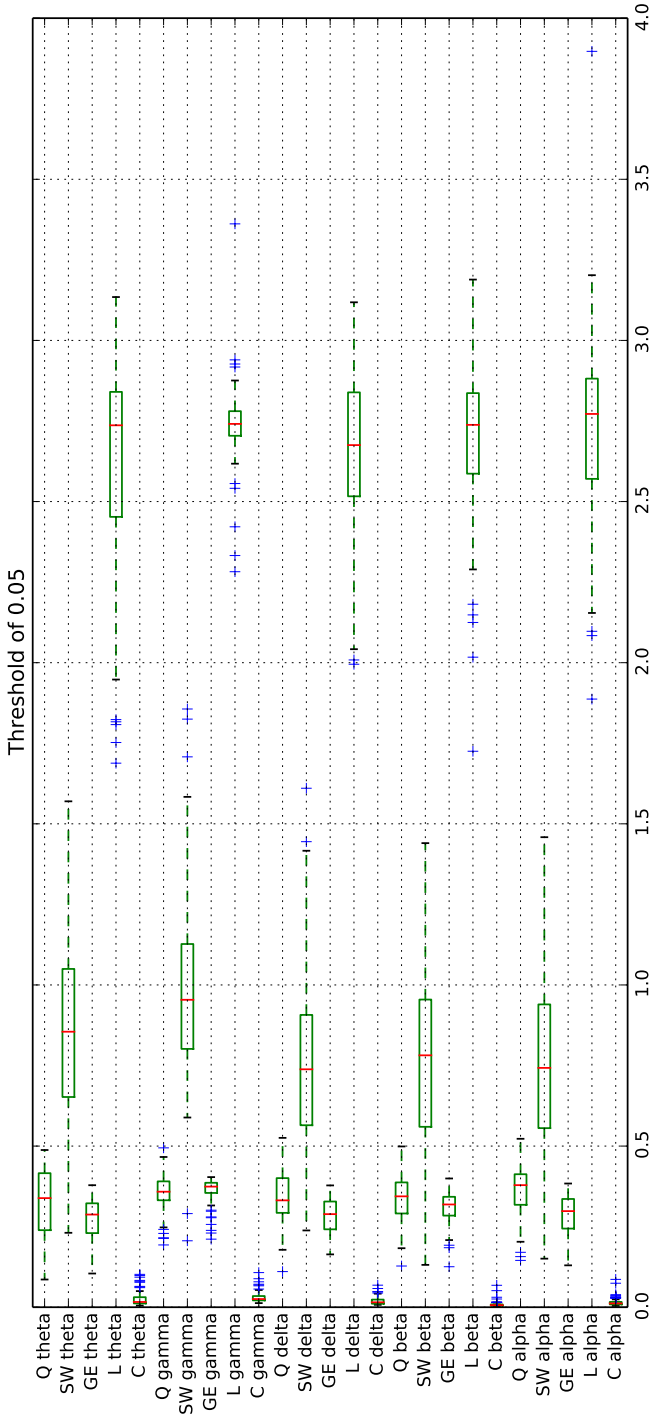

Figure A.2: Box plot of graph measures for threshold 0.05.

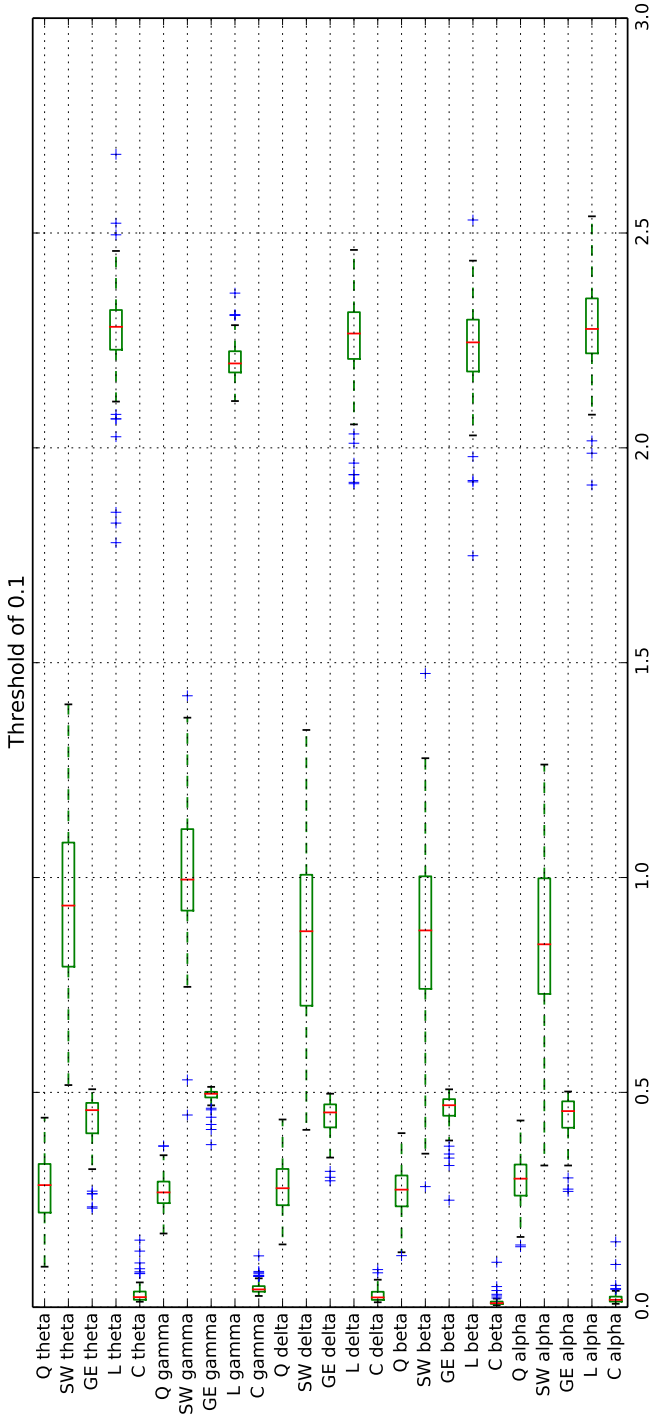

Figure A.3: Box plot of graph measures for threshold 0.1.

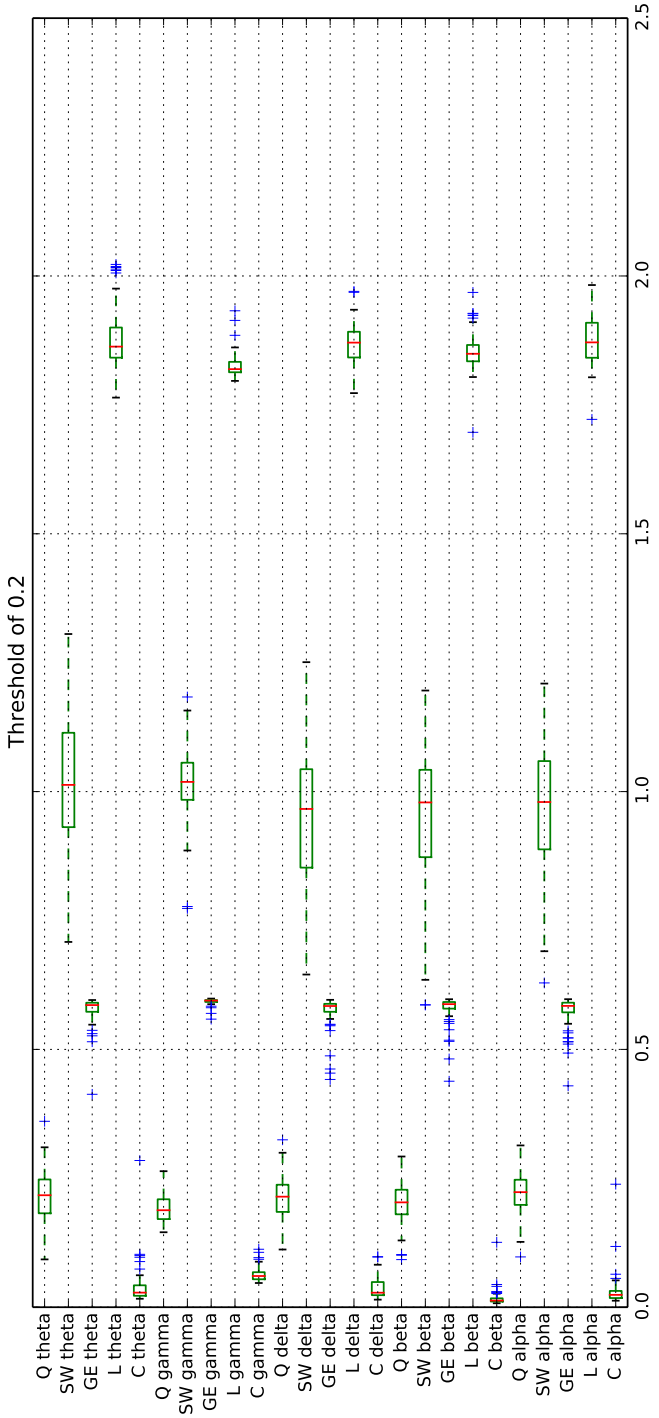

Figure A.4: Box plot of graph measures for threshold 0.2.

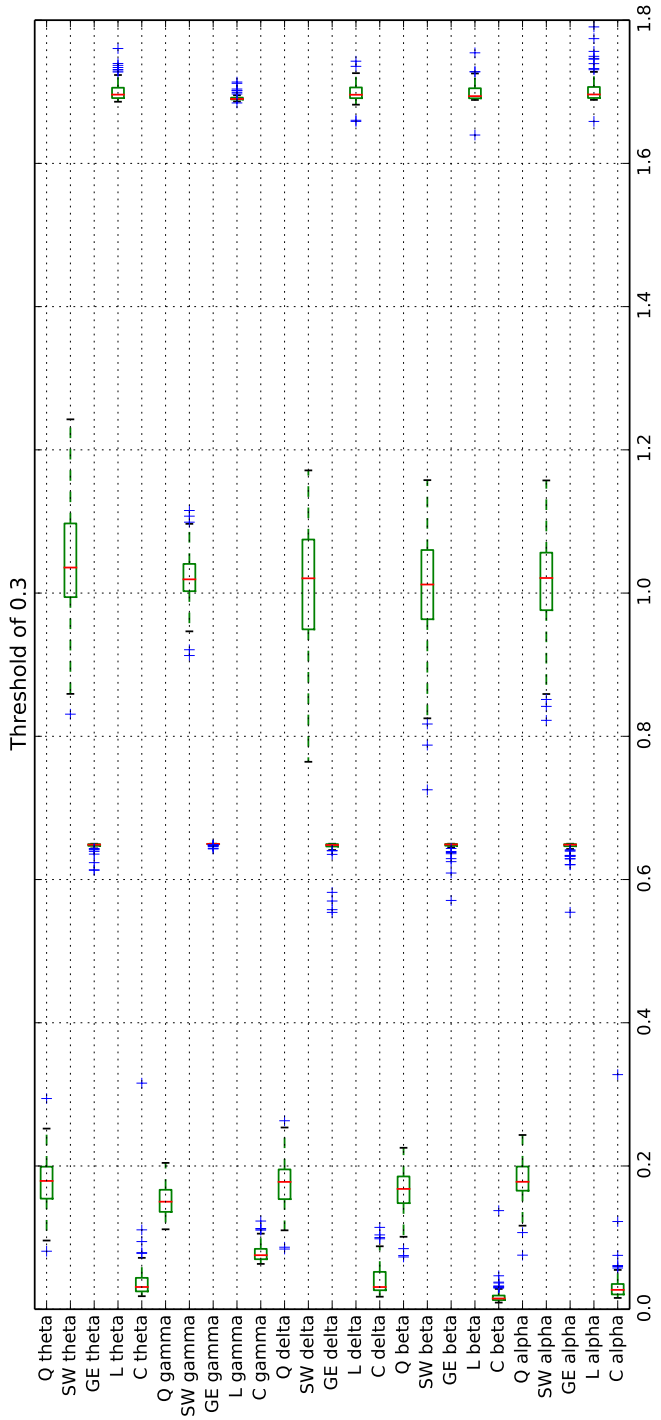

Figure A.5: Box plot of graph measures for threshold 0.3.

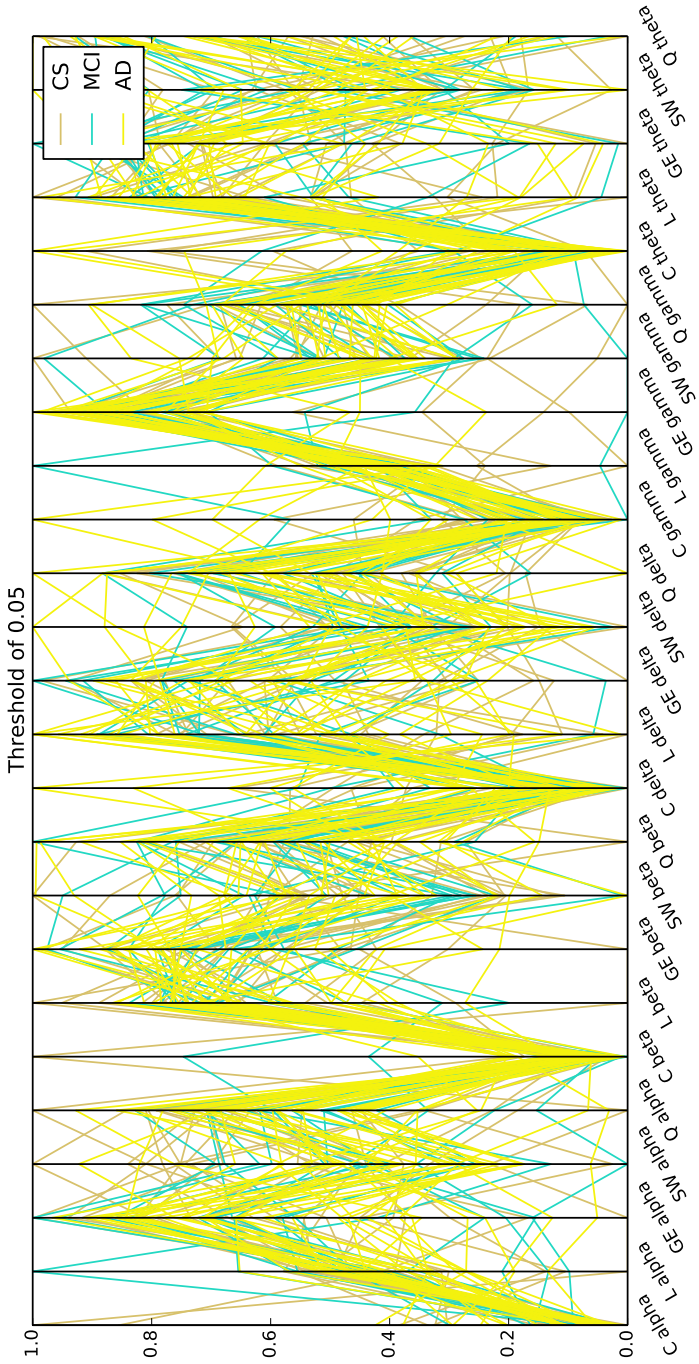

Figure A.6: Parallel coordinates plot of graph measures for threshold 0.05.

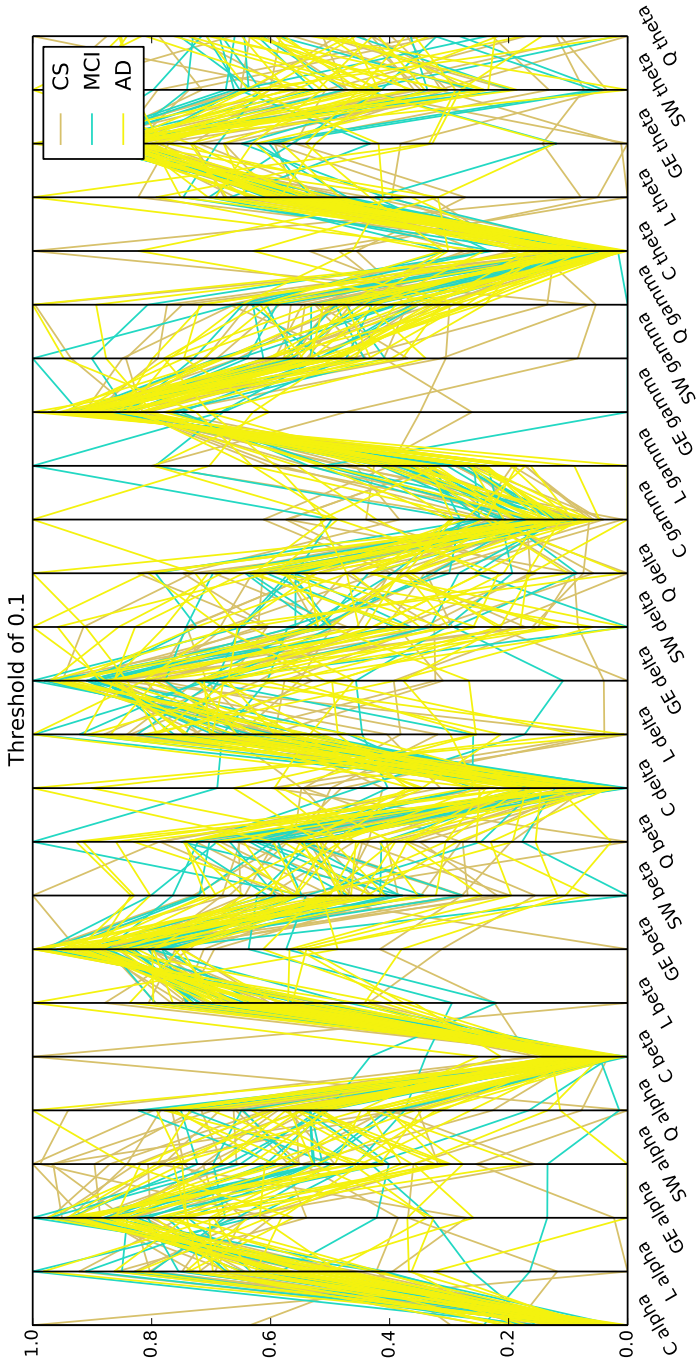

Figure A.7: Parallel coordinates plot of graph measures for threshold 0.1.

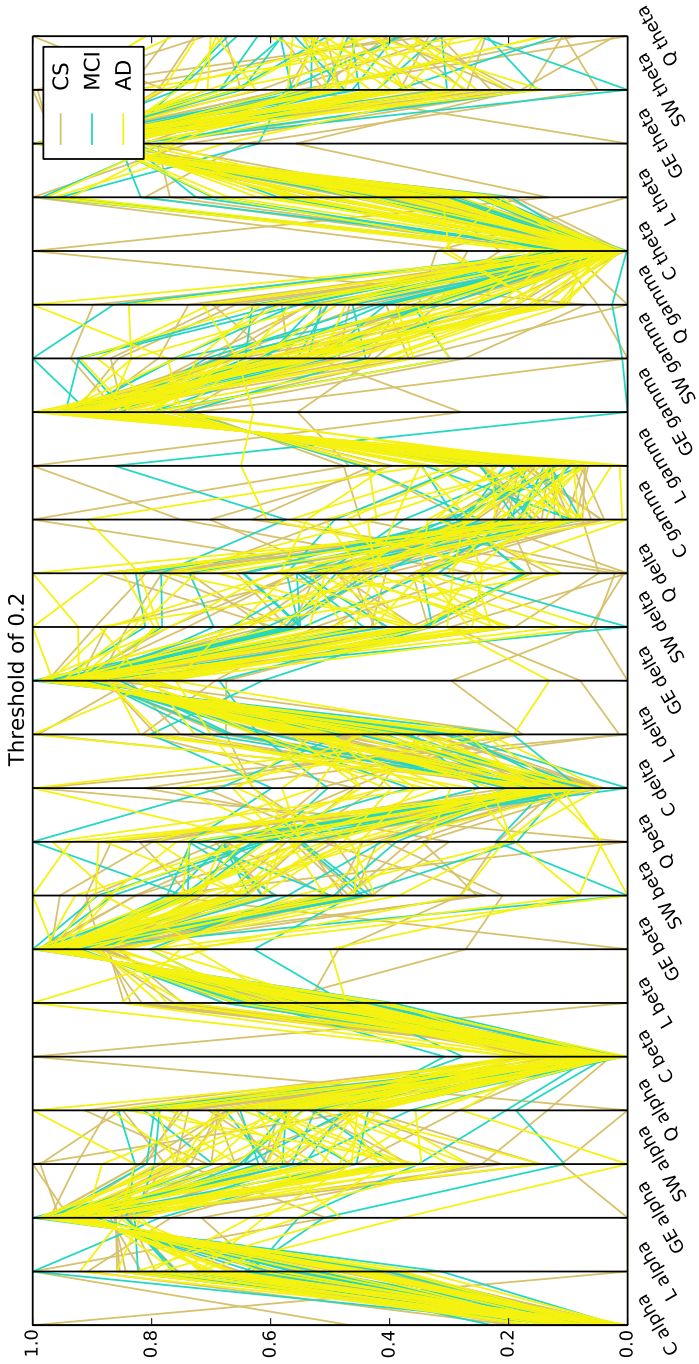

Figure A.8: Parallel coordinates plot of graph measures for threshold 0.2.

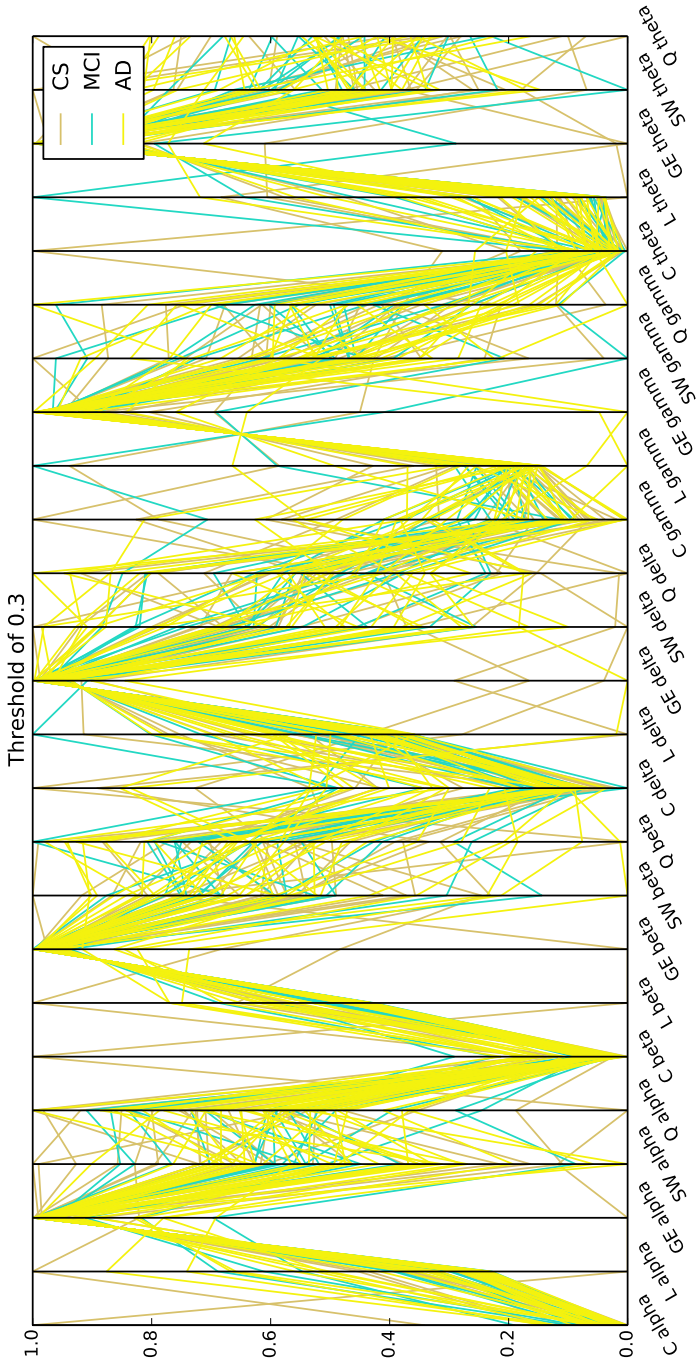

Figure A.9: Parallel coordinates plot of graph measures for threshold 0.3.

Appendix B

Statistical Analysis

Table B.1: Results of the FDA statistics. Entries are sorted in ascending order according to their p-values.

Measure	**Group A**	**Group B**	**Band**	**p-value**
SW	CS	AD	alpha	0.006
SW	CS	MCI	alpha	0.0657
GE	CS	MCI	delta	0.161
L	CS	MCI	delta	0.1637
Q	CS	MCI	beta	0.1688
L	CS	AD	gamma	0.1691
GE	CS	MCI	beta	0.1868
L	CS	AD	theta	0.1902
Q	MCI	AD	beta	0.1907
Q	CS	AD	theta	0.1912
C	MCI	AD	theta	0.1914
C	CS	MCI	theta	0.1942
GE	CS	AD	gamma	0.2103
C	MCI	AD	delta	0.2203
GE	MCI	AD	gamma	0.2224
L	CS	MCI	theta	0.226
C	CS	AD	alpha	0.2401
GE	CS	AD	beta	0.2445
GE	CS	AD	delta	0.252

Continued on next page

Table B.1 – continued from previous page

Measure	Group A	Group B	Band	p-value
Q	CS	AD	delta	0.2991
Q	CS	MCI	delta	0.3342
Q	MCI	AD	gamma	0.3437
L	CS	AD	delta	0.3471
L	MCI	AD	gamma	0.3492
L	CS	MCI	gamma	0.358
L	MCI	AD	alpha	0.3704
GE	CS	MCI	theta	0.3777
Q	CS	MCI	theta	0.4293
GE	CS	AD	theta	0.4317
C	CS	MCI	alpha	0.4711
GE	MCI	AD	delta	0.4861
C	CS	AD	theta	0.4919
C	CS	MCI	delta	0.5119
SW	CS	AD	beta	0.5163
SW	CS	AD	gamma	0.551
Q	CS	MCI	alpha	0.5597
Q	CS	AD	gamma	0.5603
C	MCI	AD	gamma	0.5662
SW	MCI	AD	alpha	0.6005
Q	CS	AD	alpha	0.6031
GE	MCI	AD	theta	0.6147
C	CS	AD	delta	0.6189
L	MCI	AD	delta	0.6314
GE	MCI	AD	beta	0.6318
L	CS	AD	alpha	0.6667
SW	MCI	AD	gamma	0.6716
SW	CS	MCI	beta	0.7291
Q	CS	MCI	gamma	0.7329
Q	MCI	AD	theta	0.7575
L	MCI	AD	theta	0.7618
SW	CS	MCI	delta	0.793

Continued on next page

Table B.1 – continued from previous page

Measure	Group A	Group B	Band	p-value
L	CS	MCI	beta	0.812
C	CS	AD	gamma	0.825
L	CS	MCI	alpha	0.8289
C	MCI	AD	beta	0.8313
SW	CS	AD	theta	0.8538
L	CS	AD	beta	0.8565
C	CS	MCI	gamma	0.8794
SW	MCI	AD	theta	0.887
SW	CS	MCI	theta	0.8873
SW	MCI	AD	beta	0.8953
SW	MCI	AD	delta	0.8966
C	MCI	AD	alpha	0.9096
Q	MCI	AD	alpha	0.9125
C	CS	MCI	beta	0.9171
GE	MCI	AD	alpha	0.9308
C	CS	AD	beta	0.9354
GE	CS	AD	alpha	0.9372
GE	CS	MCI	gamma	0.9539
SW	CS	MCI	gamma	0.9549
SW	CS	AD	delta	0.9622
L	MCI	AD	beta	0.9775
GE	CS	MCI	alpha	0.9853
Q	MCI	AD	delta	0.9858
Q	CS	AD	beta	0.9938

Appendix C

Confusion Matrices

C.1 Logistic Regression

		Predicted Class		
		CS	MCI	AD
Actual Class	CS	13	2	11
	MCI	4	3	11
	AD	10	3	23

Table C.1: Confusion matrix for logistic regression trained on original data, threshold 0.05.

		Predicted Class		
		CS	MCI	AD
Actual Class	CS	25	4	7
	MCI	7	20	9
	AD	8	11	17

Table C.2: Confusion matrix for logistic regression trained on data with SMOTE, threshold 0.05.

		Predicted Class		
		CS	MCI	AD
Actual Class	CS	13	3	10
	MCI	6	2	10
	AD	9	6	21

Table C.3: Confusion matrix for logistic regression trained on original data, threshold 0.1.

		Predicted Class		
		CS	MCI	AD
Actual Class	CS	24	5	7
	MCI	8	21	7
	AD	10	9	17

Table C.4: Confusion matrix for logistic regression trained on data with SMOTE, threshold 0.1.

		Predicted Class		
		CS	MCI	AD
Actual Class	CS	10	4	12
	MCI	5	2	11
	AD	9	5	22

Table C.5: Confusion matrix for logistic regression trained on original data, threshold 0.15.

		Predicted Class		
		CS	MCI	AD
Actual Class	CS	15	11	10
	MCI	11	17	8
	AD	11	10	15

Table C.6: Confusion matrix for logistic regression trained on data with SMOTE, threshold 0.15.

		Predicted Class		
		CS	MCI	AD
Actual Class	CS	9	5	12
	MCI	5	0	13
	AD	9	6	21

Table C.7: Confusion matrix for logistic regression trained on original data, threshold 0.2.

		Predicted Class		
		CS	MCI	AD
Actual Class	CS	21	7	8
	MCI	4	20	12
	AD	10	13	13

Table C.8: Confusion matrix for logistic regression trained on data with SMOTE, threshold 0.2.

		Predicted Class		
		CS	MCI	AD
Actual Class	CS	6	6	14
	MCI	6	2	10
	AD	10	4	22

Table C.9: Confusion matrix for logistic regression trained on original data, threshold 0.3.

		Predicted Class		
		CS	MCI	AD
Actual Class	CS	13	13	10
	MCI	12	11	13
	AD	6	11	19

Table C.10: Confusion matrix for logistic regression trained on data with SMOTE, threshold 0.3.

C.2 Random Forest

		Predicted Class		
		CS	MCI	AD
Actual Class	CS	10	2	14
	MCI	4	2	12
	AD	7	1	28

Table C.11: Confusion matrix for random forest trained on original data, threshold 0.05.

		Predicted Class		
		CS	MCI	AD
Actual Class	CS	21	1	8
	MCI	1	28	7
	AD	6	10	20

Table C.12: Confusion matrix for random forest trained on data with SMOTE, threshold 0.05.

		Predicted Class		
		CS	MCI	AD
Actual Class	CS	8	2	16
	MCI	3	1	14
	AD	7	3	26

Table C.13: Confusion matrix for random forest trained on original data, threshold 0.1.

		Predicted Class		
		CS	MCI	AD
Actual Class	CS	25	6	5
	MCI	1	31	4
	AD	7	10	19

Table C.14: Confusion matrix for random forest trained on data with SMOTE, threshold 0.1.

		Predicted Class		
		CS	MCI	AD
Actual Class	CS	10	1	15
	MCI	3	0	15
	AD	9	1	26

Table C.15: Confusion matrix for random forest trained on original data, threshold 0.15.

		Predicted Class		
		CS	MCI	AD
Actual Class	CS	25	3	8
	MCI	2	29	5
	AD	8	7	21

Table C.16: Confusion matrix for random forest trained on data with SMOTE, threshold 0.15.

		Predicted Class		
		CS	MCI	AD
Actual Class	CS	6	2	18
	MCI	3	0	15
	AD	7	1	28

Table C.17: Confusion matrix for random forest trained on original data, threshold 0.2.

		Predicted Class		
		CS	MCI	AD
Actual Class	CS	24	4	8
	MCI	2	29	5
	AD	6	10	20

Table C.18: Confusion matrix for random forest trained on data with SMOTE, threshold 0.2.

		Predicted Class		
		CS	MCI	AD
Actual Class	CS	12	0	14
	MCI	3	0	15
	AD	6	1	29

Table C.19: Confusion matrix for random forest trained on original data, threshold 0.3.

		Predicted Class		
		CS	MCI	AD
Actual Class	CS	23	6	7
	MCI	4	26	6
	AD	7	8	21

Table C.20: Confusion matrix for random forest trained on data with SMOTE, threshold 0.3.

Bibliography

Achard, S. and Bullmore, E. (2007) 'Efficiency and cost of economical brain functional networks.', *PLoS computational biology* 3 (2), e17, ISSN: 1553-7358, DOI: 10.1371/journal.pcbi.0030017.

Andrews-Hanna, J.R., Reidler, J.S., Sepulcre, J., Poulin, R. and Buckner, R.L. (2010) 'Functional-anatomic fractionation of the brain's default network.', *Neuron* 65 (4), pp. 550–62, ISSN: 1097-4199, DOI: 10.1016/j.neuron.2010.02.005.

Aydore, S., Pantazis, D. and Leahy, R.M. (2013) 'A note on the phase locking value and its properties.', *NeuroImage* 74, pp. 231–44, ISSN: 1095-9572, DOI: 10.1016/j.neuroimage.2013.02.008.

Bassett, D.S., Nelson, B.G., Mueller, B.A., Camchong, J. and Lim, K.O. (2012) 'Altered resting state complexity in schizophrenia.', *NeuroImage* 59 (3), pp. 2196–207, ISSN: 1095-9572, DOI: 10.1016/j.neuroimage.2011.10.002.

Bassett, D.S., Nelson, B.G., Mueller, B.a., Camchong, J. and Lim, K.O. (2012) 'Altered resting state complexity in schizophrenia.', *NeuroImage* 59 (3), pp. 2196–207, ISSN: 1095-9572, DOI: 10.1016/j.neuroimage.2011.10.002.

Beckmann, C.F., DeLuca, M., Devlin, J.T. and Smith, S.M. (2005) 'Investigations into resting-state connectivity using independent component analysis.', *Philosophical transactions of the Royal Society of London. Series B, Biological sciences* 360 (1457), pp. 1001–13, ISSN: 0962-8436, DOI: 10.1098/rstb.2005.1634.

Breiman, L. (2001) 'Random forests', *Machine learning* 45 (1), pp. 5–32.

Brookmeyer, R., Johnson, E., Ziegler-Graham, K. and Arrighi, H.M. (2007) 'Forecasting the global burden of Alzheimer's disease.', *Alzheimer's & dementia :*

the journal of the Alzheimer's Association 3 (3), pp. 186–91, ISSN: 1552-5279, DOI: 10.1016/j.jalz.2007.04.381.

Bullmore, E. and Sporns, O. (2009) 'Complex brain networks: graph theoretical analysis of structural and functional systems.', *Nature reviews. Neuroscience* 10 (3), pp. 186–98, ISSN: 1471-0048, DOI: 10.1038/nrn2575.

Bullmore, E.T. and Bassett, D.S. (2011) 'Brain graphs: graphical models of the human brain connectome.', *Annual review of clinical psychology* 7, pp. 113–40, ISSN: 1548-5951, DOI: 10.1146/annurev-clinpsy-040510-143934.

Chawla, N.V., Bowyer, K.W., Hall, L.O. and Kegelmeyer, W.P. (2002) 'SMOTE: Synthetic Minority Over-sampling Technique', *J. Artif. Int. Res.* 16 (1), pp. 321–357, ISSN: 1076-9757.

Chen, G., Ward, B.D., Xie, C., Li, W., Wu, Z., Jones, J.L., Franczak, M., Antuono, P. and Li, S.-J. (2011) 'Classification of Alzheimer disease, mild cognitive impairment, and normal cognitive status with large-scale network analysis based on resting-state functional MR imaging.', *Radiology* 259 (1), pp. 213–21, ISSN: 1527-1315, DOI: 10.1148/radiol.10100734.

Cohen, D. (1972) 'Magnetoencephalography: detection of the brain's electrical activity with a superconducting magnetometer.', *Science (New York, N.Y.)* 175 (4022), pp. 664–6, ISSN: 0036-8075.

Cummings, J.L. (2004) 'Alzheimer's disease.', *The New England journal of medicine* 351 (1), pp. 56–67, ISSN: 1533-4406, DOI: 10.1056/NEJMra040223.

Damoiseaux, J.S., Rombouts, S.A.R.B., Barkhof, F., Scheltens, P., Stam, C.J., Smith, S.M. and Beckmann, C.F. (2006) 'Consistent resting-state networks across healthy subjects.', *Proceedings of the National Academy of Sciences of the United States of America* 103 (37), pp. 13848–53, ISSN: 0027-8424, DOI: 10.1073/pnas.0601417103.

De Haan, W., van der Flier, W.M., Koene, T., Smits, L.L., Scheltens, P. and Stam, C.J. (2012) 'Disrupted modular brain dynamics reflect cognitive dysfunction in Alzheimer's disease.', *NeuroImage* 59 (4), pp. 3085–93, ISSN: 1095-9572, DOI: 10.1016/j.neuroimage.2011.11.055.

De Haan, W., van der Flier, W.M., Wang, H., Van Mieghem, P.F.A., Scheltens, P. and Stam, C.J. (2012) 'Disruption of functional brain networks in Alzheimer's disease: what can we learn from graph spectral analysis of resting-state magnetoencephalography?', *Brain connectivity* 2 (2), pp. 45–55, ISSN: 2158-0022, DOI: 10.1089/brain.2011.0043.

Escudero, J., Hornero, R., Abásolo, D. and Fernández, A. (2011) 'Quantitative evaluation of artifact removal in real magnetoencephalogram signals with blind source separation.', *Annals of biomedical engineering* 39 (8), pp. 2274–86, ISSN: 1573-9686, DOI: 10.1007/s10439-011-0312-7.

Escudero, J., Sanei, S., Jarchi, D., Abásolo, D. and Hornero, R. (2011) 'Regional coherence evaluation in mild cognitive impairment and Alzheimer's disease based on adaptively extracted magnetoencephalogram rhythms.', *Physiological measurement* 32 (8), pp. 1163–80, ISSN: 1361-6579, DOI: 10.1088/0967-3334/32/8/011.

Fabisch, A. (2014) *t-SNE in sklearn (http://git.io/1Da7nQ)*.

Fallani, F.D.V., Richiardi, J., Chavez, M. and Achard, S. (2014) 'Graph analysis of functional brain networks: practical issues in translational neuroscience', *arXiv preprint arXiv:1406.7391*, arXiv: 1406.7391.

Filippi, M. and Agosta, F. (2011) 'Structural and functional network connectivity breakdown in Alzheimer's disease studied with magnetic resonance imaging techniques.', *Journal of Alzheimer's disease : JAD* 24 (3), pp. 455–74, ISSN: 1875-8908, DOI: 10.3233/JAD-2011-101854.

Folstein, M.F., Folstein, S.E. and McHugh, P.R. (1975) '"Mini-mental state". A practical method for grading the cognitive state of patients for the clinician.', *Journal of psychiatric research* 12 (3), pp. 189–98, ISSN: 0022-3956, DOI: 10.1016/0022-3956(75)90026-6.

Friston, K.J. (1994) 'Functional and effective connectivity in neuroimaging: A synthesis', *Human Brain Mapping* 2 (1-2), pp. 56–78, ISSN: 10659471, DOI: 10.1002/hbm.460020107.

Gray, K.R., Aljabar, P., Heckemann, R.a., Hammers, A. and Rueckert, D. (2013) 'Random forest-based similarity measures for multi-modal classification of

Alzheimer's disease.', *NeuroImage* 65, pp. 167–75, ISSN: 1095-9572, DOI: 10.1016/j.neuroimage.2012.09.065.

Greicius, M.D., Srivastava, G., Reiss, A.L. and Menon, V. (2004) 'Default-mode network activity distinguishes Alzheimer's disease from healthy aging: evidence from functional MRI.', *Proceedings of the National Academy of Sciences of the United States of America* 101 (13), pp. 4637–42, ISSN: 0027-8424, DOI: 10.1073/pnas.0308627101.

Gross, J., Baillet, S., Barnes, G.R., Henson, R.N., Hillebrand, A., Jensen, O., Jerbi, K., Litvak, V., Maess, B., Oostenveld, R., Parkkonen, L., Taylor, J.R., van Wassenhove, V., Wibral, M. and Schoffelen, J.-M. (2013) 'Good practice for conducting and reporting MEG research.', *NeuroImage* 65, pp. 349–63, ISSN: 1095-9572, DOI: 10.1016/j.neuroimage.2012.10.001.

Gusnard, D.A. and Raichle, M.E. (2001) 'Searching for a baseline: functional imaging and the resting human brain.', *Nature reviews. Neuroscience* 2 (10), pp. 685–94, ISSN: 1471-003X, DOI: 10.1038/35094500.

He, Y., Chen, Z., Gong, G. and Evans, A. (2009) 'Neuronal networks in Alzheimer's disease.', *The Neuroscientist : a review journal bringing neurobiology, neurology and psychiatry* 15 (4), pp. 333–50, ISSN: 1073-8584, DOI: 10.1177/1073858409334423.

Hoogenboom, N., Schoffelen, J.-M., Oostenveld, R., Parkes, L.M. and Fries, P. (2006) 'Localizing human visual gamma-band activity in frequency, time and space.', *NeuroImage* 29 (3), pp. 764–73, ISSN: 1053-8119, DOI: 10.1016/j.neuroimage.2005.08.043.

Hornero, R., Escudero, J., Fernández, A., Poza, J. and Gómez, C. (2008) 'Spectral and nonlinear analyses of MEG background activity in patients with Alzheimer's disease.', *IEEE transactions on bio-medical engineering* 55 (6), pp. 1658–65, ISSN: 0018-9294.

I-LABS (2014) *Origin of the MEG Signal. From http://ilabs.washington.edu/what-magnetoencephalography-meg.*

Jeschkies, K. (2012) *Python implementation of SMOTE (http://git.io/xy0JwA).*

Jie, B., Zhang, D., Wee, C.-Y. and Shen, D. (2014) 'Topological graph kernel on multiple thresholded functional connectivity networks for mild cognitive impairment classification.', *Human brain mapping* 35 (7), pp. 2876–97, ISSN: 1097-0193, DOI: 10.1002/hbm.22353.

Jones, D.K. and Leemans, A. (2011) 'Diffusion tensor imaging.', *Methods in molecular biology (Clifton, N.J.)* 711, pp. 127–44, ISSN: 1940-6029, DOI: 10.1007/978-1-61737-992-5_6.

Jousmäki, V. and Hari, R. (1996) 'Cardiac artifacts in magnetoencephalogram.', *Journal of clinical neurophysiology : official publication of the American Electroencephalographic Society* 13 (2), pp. 172–6, ISSN: 0736-0258.

Keshtkaran, M.R. and Yang, Z. (2014) 'A fast, robust algorithm for power line interference cancellation in neural recording.', *Journal of neural engineering* 11 (2), p. 026017, ISSN: 1741-2552, DOI: 10.1088/1741-2560/11/2/026017.

Khachaturian, Z.S. (1985) 'Diagnosis of Alzheimer's Disease', *Archives of Neurology* 42 (11), pp. 1097–1105, ISSN: 0003-9942, DOI: 10.1001/archneur.1985.04060100083029.

Lachaux, J.P., Rodriguez, E., Martinerie, J. and Varela, F.J. (1999) 'Measuring phase synchrony in brain signals.', *Human brain mapping* 8 (4), pp. 194–208, ISSN: 1065-9471.

Lalkhen, A.G. and McCluskey, A. (2008) 'Clinical tests: sensitivity and specificity', *Continuing Education in Anaesthesia, Critical Care & Pain* 8 (6), pp. 221–223, DOI: 10.1093/bjaceaccp/mkn041.

Latora, V. and Marchiori, M. (2001) 'Efficient Behavior of Small-World Networks', *Physical Review Letters* 87 (19), p. 198701, ISSN: 0031-9007, DOI: 10.1103/PhysRevLett.87.198701.

Le Van Quyen, M., Foucher, J., Lachaux, J., Rodriguez, E., Lutz, A., Martinerie, J. and Varela, F.J. (2001) 'Comparison of Hilbert transform and wavelet methods for the analysis of neuronal synchrony.', *Journal of neuroscience methods* 111 (2), pp. 83–98, ISSN: 0165-0270.

Lehmann, C., Koenig, T., Jelic, V., Prichep, L., John, R.E., Wahlund, L.-O., Dodge, Y. and Dierks, T. (2007) 'Application and comparison of classification

algorithms for recognition of Alzheimer's disease in electrical brain activity (EEG).', *Journal of neuroscience methods* 161 (2), pp. 342–50, ISSN: 0165-0270, DOI: 10.1016/j.jneumeth.2006.10.023.

Lo, C.-Y., Wang, P.-N., Chou, K.-H., Wang, J., He, Y. and Lin, C.-P. (2010) 'Diffusion tensor tractography reveals abnormal topological organization in structural cortical networks in Alzheimer's disease.', *The Journal of neuroscience : the official journal of the Society for Neuroscience* 30 (50), pp. 16876–85, ISSN: 1529-2401, DOI: 10.1523/JNEUROSCI.4136-10.2010.

Lopes da Silva, F. (2013) 'EEG and MEG: relevance to neuroscience.', *Neuron* 80 (5), pp. 1112–28, ISSN: 1097-4199, DOI: 10.1016/j.neuron.2013.10.017.

Maaten, L.V.D. and Hinton, G. (2008) 'Visualizing data using t-SNE', *Journal of Machine Learning Research* 9, pp. 2579–2605.

Mitra, P.P. and Pesaran, B. (1999) 'Analysis of dynamic brain imaging data.', *Biophysical journal* 76 (2), pp. 691–708, ISSN: 0006-3495, DOI: 10.1016/S0006-3495(99)77236-X.

Morris, J.C., Storandt, M., Miller, J.P., McKeel, D.W., Price, J.L., Rubin, E.H. and Berg, L. (2001) 'Mild cognitive impairment represents early-stage Alzheimer disease.', *Archives of neurology* 58 (3), pp. 397–405, ISSN: 0003-9942.

Murphy, K.P. (2012) *Machine Learning: A Probabilistic Perspective*, The MIT Press, ISBN: 0262018020, 9780262018029.

Newman, M. and Girvan, M. (2004) 'Finding and evaluating community structure in networks', *Physical Review E* 69 (2), p. 026113, ISSN: 1539-3755, DOI: 10.1103/PhysRevE.69.026113, arXiv: 0308217 [cond-mat].

Nolte, G., Bai, O., Wheaton, L., Mari, Z., Vorbach, S. and Hallett, M. (2004) 'Identifying true brain interaction from EEG data using the imaginary part of coherency.', *Clinical neurophysiology : official journal of the International Federation of Clinical Neurophysiology* 115 (10), pp. 2292–307, ISSN: 1388-2457, DOI: 10.1016/j.clinph.2004.04.029.

Oostenveld, R., Fries, P., Maris, E. and Schoffelen, J.-M. (2011) 'FieldTrip: Open source software for advanced analysis of MEG, EEG, and invasive electro-

physiological data.', *Computational intelligence and neuroscience* 2011, p. 156869, ISSN: 1687-5273, DOI: 10.1155/2011/156869.

Pedregosa, F., Varoquaux, G., Gramfort, A., Michel, V., Thirion, B., Grisel, O., Blondel, M., Prettenhofer, P., Weiss, R., Dubourg, V., Vanderplas, J., Passos, A., Cournapeau, D., Brucher, M., Perrot, M. and Duchesnay, É. (2011) 'Scikit-learn: Machine Learning in Python', *J. Mach. Learn. Res.* 12, pp. 2825–2830, ISSN: 1532-4435.

Percival, D.B. and Walden, A.T. (1993) *Spectral Analysis for Physical Applications: Multitaper and Conventional Univariate Techniques*, Cambridge: Cambridge University Press, ISBN: 9780511622762, DOI: 10.1017/CBO9780511622762.

Raichle, M.E., MacLeod, a.M., Snyder, a.Z., Powers, W.J., Gusnard, D.a. and Shulman, G.L. (2001) 'A default mode of brain function.', *Proceedings of the National Academy of Sciences of the United States of America* 98 (2), pp. 676–82, ISSN: 0027-8424, DOI: 10.1073/pnas.98.2.676.

Ramsay, J. and Silverman, B.W. (2005) *Functional Data Analysis*, 2nd, Springer, ISBN: 978-0-387-22751-1.

Richiardi, J., Achard, S., Bunke, H. and Van De Ville, D. (2013) 'Machine Learning with Brain Graphs: Predictive Modeling Approaches for Functional Imaging in Systems Neuroscience', *IEEE Signal Processing Magazine* 30 (3), pp. 58–70, ISSN: 1053-5888, DOI: 10.1109/MSP.2012.2233865.

Rowe, J.B., Hughes, L.E., Barker, R.A. and Owen, A.M. (2010) 'Dynamic causal modelling of effective connectivity from fMRI: are results reproducible and sensitive to Parkinson's disease and its treatment?', *NeuroImage* 52 (3), pp. 1015–26, ISSN: 1095-9572, DOI: 10.1016/j.neuroimage.2009.12.080.

Rubinov, M. and Sporns, O. (2010) 'Complex network measures of brain connectivity: uses and interpretations.', *NeuroImage* 52 (3), pp. 1059–69, ISSN: 1095-9572, DOI: 10.1016/j.neuroimage.2009.10.003.

Rudie, J.D., Brown, J.a., Beck-Pancer, D., Hernandez, L.M., Dennis, E.L., Thompson, P.M., Bookheimer, S.Y. and Dapretto, M. (2012) 'Altered functional and structural brain network organization in autism.', *NeuroImage. Clinical* 2, pp. 79–94, ISSN: 2213-1582, DOI: 10.1016/j.nicl.2012.11.006.

Schnitzler, A. and Gross, J. (2005) 'Normal and pathological oscillatory communication in the brain.', *Nature reviews. Neuroscience* 6 (4), pp. 285–96, ISSN: 1471-003X, DOI: 10.1038/nrn1650.

Schoffelen, J.-M. and Gross, J. (2009) 'Source connectivity analysis with MEG and EEG.', *Human brain mapping* 30 (6), pp. 1857–65, ISSN: 1097-0193, DOI: 10.1002/hbm.20745.

Sheline, Y.I., Raichle, M.E., Snyder, A.Z., Morris, J.C., Head, D., Wang, S. and Mintun, M.a. (2010) 'Amyloid plaques disrupt resting state default mode network connectivity in cognitively normal elderly.', *Biological psychiatry* 67 (6), pp. 584–7, ISSN: 1873-2402, DOI: 10.1016/j.biopsych.2009.08.024.

Slepian, D. (1978) 'Prolate spheroidal wave functions, Fourier analysis, and uncertainty—V: The discrete case', *Bell System Technical Journal* 57 (5), pp. 1371–1430.

Smith, S.W. (1997) *The scientist and engineer's guide to digital signal processing*, California Technical Pub. San Diego, pp. 261–270, ISBN: 0966017676.

Sperling, R.a., Aisen, P.S., Beckett, L.a., Bennett, D.a., Craft, S., Fagan, A.M., Iwatsubo, T., Jack, C.R., Kaye, J., Montine, T.J., Park, D.C., Reiman, E.M., Rowe, C.C., Siemers, E., Stern, Y., Yaffe, K., Carrillo, M.C., Thies, B., Morrison-Bogorad, M., Wagster, M.V. and Phelps, C.H. (2011) 'Toward defining the preclinical stages of Alzheimer's disease: recommendations from the National Institute on Aging-Alzheimer's Association workgroups on diagnostic guidelines for Alzheimer's disease.', *Alzheimer's & dementia : the journal of the Alzheimer's Association* 7 (3), pp. 280–92, ISSN: 1552-5279, DOI: 10.1016/j.jalz.2011.03.003.

Sporns, O. (2011) *Networks of the Brain*, MIT press.

Stam, C.J. (2004) 'Functional connectivity patterns of human magnetoencephalographic recordings: a 'small-world' network?', *Neuroscience letters* 355 (1-2), pp. 25–8, ISSN: 0304-3940, DOI: 10.1016/j.neulet.2003.10.063.

Stam, C.J. (2010) 'Use of magnetoencephalography (MEG) to study functional brain networks in neurodegenerative disorders.', *Journal of the neurological sciences* 289 (1-2), pp. 128–34, ISSN: 1878-5883, DOI: 10.1016/j.jns.2009.08.028.

Stam, C.J., de Haan, W., Daffertshofer, A., Jones, B.F., Manshanden, I., van Cappellen van Walsum, A.M., Montez, T., Verbunt, J.P.a., de Munck, J.C., van Dijk, B.W., Berendse, H.W. and Scheltens, P. (2009) 'Graph theoretical analysis of magnetoencephalographic functional connectivity in Alzheimer's disease.', *Brain : a journal of neurology* 132 (Pt 1), pp. 213–24, ISSN: 1460-2156, DOI: 10.1093/brain/awn262.

Stam, C.J., Jones, B.F., Manshanden, I., van Cappellen van Walsum, a.M., Montez, T., Verbunt, J.P.a., de Munck, J.C., van Dijk, B.W., Berendse, H.W. and Scheltens, P. (2006) 'Magnetoencephalographic evaluation of resting-state functional connectivity in Alzheimer's disease.', *NeuroImage* 32 (3), pp. 1335–44, ISSN: 1053-8119, DOI: 10.1016/j.neuroimage.2006.05.033.

Stam, C.J., Jones, B.F., Nolte, G., Breakspear, M. and Scheltens, P. (2007) 'Small-world networks and functional connectivity in Alzheimer's disease.', *Cerebral cortex (New York, N.Y. : 1991)* 17 (1), pp. 92–9, ISSN: 1047-3211, DOI: 10.1093/cercor/bhj127.

Stam, C.J., Tewarie, P., Van Dellen, E., van Straaten, E.C.W., Hillebrand, A. and Van Mieghem, P. (2014) 'The trees and the forest: Characterization of complex brain networks with minimum spanning trees.', *International journal of psychophysiology : official journal of the International Organization of Psychophysiology* 92 (3), pp. 129–38, ISSN: 1872-7697, DOI: 10.1016/j.ijpsycho.2014.04.001.

Stam, C.J. and van Straaten, E.C.W. (2012) 'The organization of physiological brain networks.', *Clinical neurophysiology : official journal of the International Federation of Clinical Neurophysiology* 123 (6), pp. 1067–87, ISSN: 1872-8952, DOI: 10.1016/j.clinph.2012.01.011.

Stam, C.J., Nolte, G. and Daffertshofer, A. (2007) 'Phase lag index: assessment of functional connectivity from multi channel EEG and MEG with diminished bias from common sources.', *Human brain mapping* 28 (11), pp. 1178–93, ISSN: 1065-9471, DOI: 10.1002/hbm.20346.

Stam, C.J. and Reijneveld, J.C. (2007) 'Graph theoretical analysis of complex networks in the brain.', *Nonlinear biomedical physics* 1 (1), p. 3, ISSN: 1753-4631, DOI: 10.1186/1753-4631-1-3.

Stanciu, D. and Escudero, J. (2014) 'Analysis of Functional Brain Connectivity using Graph Theory in Alzheimer's Disease', *Summer Project Proposal*, pp. 1–12.

Tadel, F., Baillet, S., Mosher, J.C., Pantazis, D. and Leahy, R.M. (2011) 'Brainstorm: a user-friendly application for MEG/EEG analysis.', *Computational intelligence and neuroscience* 2011, p. 879716, ISSN: 1687-5273, DOI: 10.1155/2011/879716.

Tijms, B.M., Wink, A.M., de Haan, W., van der Flier, W.M., Stam, C.J., Scheltens, P. and Barkhof, F. (2013) 'Alzheimer's disease: connecting findings from graph theoretical studies of brain networks.', *Neurobiology of aging* 34 (8), pp. 2023–36, ISSN: 1558-1497, DOI: 10.1016/j.neurobiolaging.2013.02.020.

Varela, F., Lachaux, J.P., Rodriguez, E. and Martinerie, J. (2001) 'The brainweb: phase synchronization and large-scale integration.', *Nature reviews. Neuroscience* 2 (4), pp. 229–39, ISSN: 1471-003X, DOI: 10.1038/35067550.

Vinck, M., Oostenveld, R., van Wingerden, M., Battaglia, F. and Pennartz, C.M.a. (2011) 'An improved index of phase-synchronization for electrophysiological data in the presence of volume-conduction, noise and sample-size bias.', *NeuroImage* 55 (4), pp. 1548–65, ISSN: 1095-9572, DOI: 10.1016/j.neuroimage.2011.01.055.

Vindiola, M.M., Vettel, J.M., Gordon, S.M., Franaszczuk, P.J. and McDowell, K. (2014) 'Applying EEG phase synchronization measures to non-linearly coupled neural mass models.', *Journal of neuroscience methods* 226, pp. 1–14, ISSN: 1872-678X, DOI: 10.1016/j.jneumeth.2014.01.025.

Vrba, J. and Robinson, S.E. (2001) 'Signal processing in magnetoencephalography.', *Methods (San Diego, Calif.)* 25 (2), pp. 249–71, ISSN: 1046-2023, DOI: 10.1006/meth.2001.1238.

Watts, D.J. and Strogatz, S.H. (1998) 'Collective dynamics of 'small-world' networks.', *Nature* 393 (6684), pp. 440–2, ISSN: 0028-0836, DOI: 10.1038/30918.

Weiner, M.W., Veitch, D.P., Aisen, P.S., Beckett, L.a., Cairns, N.J., Green, R.C., Harvey, D., Jack, C.R., Jagust, W., Liu, E., Morris, J.C., Petersen, R.C., Saykin, A.J., Schmidt, M.E., Shaw, L., Shen, L., Siuciak, J.a., Soares, H.,

Toga, A.W. and Trojanowski, J.Q. (2013) 'The Alzheimer's Disease Neuroimaging Initiative: a review of papers published since its inception.', *Alzheimer's & dementia : the journal of the Alzheimer's Association* 9 (5), e111–94, ISSN: 1552-5279, DOI: 10.1016/j.jalz.2013.05.1769.

Welch, P. (1967) 'The use of fast Fourier transform for the estimation of power spectra: a method based on time averaging over short, modified periodograms', *IEEE Transactions on audio and electroacoustics* 15.2, pp. 70–73.

Witten, I.H. and Frank, E. (2005) *Data Mining: Practical machine learning tools and techniques*, Morgan Kaufmann.

Xie, T. and He, Y. (2011) 'Mapping the Alzheimer's brain with connectomics.', *Frontiers in psychiatry* 2, p. 77, ISSN: 1664-0640, DOI: 10.3389/fpsyt.2011.00077.

Zhao, X., Liu, Y., Wang, X., Liu, B., Xi, Q., Guo, Q., Jiang, H., Jiang, T. and Wang, P. (2012) 'Disrupted small-world brain networks in moderate Alzheimer's disease: a resting-state FMRI study.', *PloS one* 7 (3), e33540, ISSN: 1932-6203, DOI: 10.1371/journal.pone.0033540.

Zhou, J., Greicius, M.D., Gennatas, E.D., Growdon, M.E., Jang, J.Y., Rabinovici, G.D., Kramer, J.H., Weiner, M., Miller, B.L. and Seeley, W.W. (2010) 'Divergent network connectivity changes in behavioural variant frontotemporal dementia and Alzheimer's disease.', *Brain : a journal of neurology* 133 (Pt 5), pp. 1352–67, ISSN: 1460-2156, DOI: 10.1093/brain/awq075.

Zhou, L., Wang, Y., Li, Y., Yap, P.-T. and Shen, D. (2011) 'Hierarchical anatomical brain networks for MCI prediction: revisiting volumetric measures.', *PloS one* 6 (7), e21935, ISSN: 1932-6203, DOI: 10.1371/journal.pone.0021935.

Zhu, J., Zou, H., Rosset, S. and Hastie, T. (2009) 'Multi-class adaboost', *Statistics and Its Interface* 2, pp. 349–360.